Non-transdermal microneedles for advanced drug delivery

KangJu Lee[a,b], **Marcus J. Goudie**[a,b], **Peyton Tebon**[a,b], **Wujin Sun**[a,b], **Zhimin Luo**[a,b], **Junmin Lee**[a,b], **Shiming Zhang**[a,b], **Kirsten Fetah**[a,b], **Han-Jun Kim**[a,b], **Yumeng Xue**[a,b], **Mohammad Ali Darabi**[a,b], **Samad Ahadian**[a,b], **Einollah Sarikhani**[a,b], **WonHyoung Ryu**[c], **Zhen Gu**[a,b,d,e], **Paul S. Weiss**[a,b,f], **Mehmet R. Dokmeci**[b,g], **Nureddin Ashammakhi**[b,g,*], **Ali Khademhosseini**[a,b,d,g,h,*]

[a]Department of Bioengineering and Center for Minimally Invasive Therapeutics (C-MIT), University of California, Los Angeles, Los Angeles, CA 90095, USA

[b]California NanoSystems Institute, University of California, Los Angeles, Los Angeles, CA 90095, USA

[c]Department of Mechanical Engineering, Yonsei University, Seoul 03722, South Korea

[d]Jonsson Comprehensive Cancer Center, University of California, Los Angeles, Los Angeles, CA 90024, USA

[e]Joint Department of Biomedical Engineering, University of North Carolina at Chapel Hill and North Carolina State University, Raleigh, NC 27695, USA

[f]Department of Chemistry and Biochemistry, Department of Materials Science and Engineering, University of California, Los Angeles, Los Angeles, CA 90095, USA

[g]Department of Radiology, University of California, Los Angeles, Los Angeles, CA 90095, USA

[h]Department of Chemical and Biomolecular Engineering, University of California, Los Angeles, Los Angeles, CA 90095, USA

Abstract

Microneedles (MNs) have been used to deliver drugs for over two decades. These platforms have been proven to increase transdermal drug delivery efficiency dramatically by penetrating restrictive tissue barriers in a minimally invasive manner. While much of the early development of MNs focused on transdermal drug delivery, this technology can be applied to a variety of other non-transdermal biomedical applications. Several variations, such as multi-layer or hollow MNs, have been developed to cater to the needs of specific applications. The heterogeneity in the design of MNs has demanded similar variety in their fabrication methods; the most common methods include micromolding and drawing lithography. Numerous materials have been explored for MN fabrication which range from biocompatible ceramics and metals to natural and synthetic biodegradable polymers. Recent advances in MN engineering have diversified MNs to include unique shapes, materials, and mechanical properties that can be tailored for organ-specific applications. In this review, we discuss the design and creation of modern MNs that aim to surpass

*Corresponding authors at: California NanoSystems Institute, University of California, Los Angeles, Los Angeles, CA 90095, USA. n.ashammakhi@ucla.edu (N.Ashammakhi), khademh@ucla.edu (A. Khademhosseini).

the biological barriers of non-transdermal drug delivery in ocular, vascular, oral, and mucosal tissue.

Keywords

Microneedle; Implant; Drug delivery; Non-transdermal; Biocompatibility; Biodegradability

1. Introduction

Conventional transdermal drug delivery is restricted by poor drug permeation through skin due to the human *stratum corneum*, which acts as a tough physical barrier [1]. Hypodermic, intradermal, and intravenous injections with rigid needles are generally used to penetrate this barrier; however, standard needles cause pain and may lead to tissue damage. Oral administration and topical drug delivery are alternatives to injection, but these result in a significant reduction in drug delivery efficiency due to first-pass elimination and/or gastrointestinal decomposition [2]. As a result, effective therapeutic drug concentrations may not always be achieved. Microneedles (MNs) have become a leading tool for transdermal drug delivery, as they have the ability to overcome the delivery efficiency issue by physically penetrating the *stratum corneum* with minimal pain and tissue damage [3,4]. One of the primary design considerations of MNs is their length; the needles must be an appropriate length to penetrate the physical barrier while also limiting damage to the tissue or other sensitive structures, such as nerves.

In 1998, the first MN arrays were developed by microfabrication, using reactive ion etching, and applied to skin to make microincisions. These MNs increased the permeability of human skin by up to 400% [5]. The safety and minimally invasive nature of MNs were also confirmed [6], and the increased permeability offered by MNs was demonstrated to facilitate the delivery of a wide range of drugs, including small [7] and large biomolecules [8,9] as well as proteins [10-13] for different applications.

MNs have been utilized for transdermal drug delivery due to their ease of use. For this reason, over the past two decades, various types of MNs have been developed. The major types include solid MNs (for puncturing tissue), drug-coated MNs, dissolvable or biodegradable MNs, and hollow MNs (Fig. 1). However, most of the work has centered around transdermal drug delivery, leaving MN-based drug delivery to other organs and tissues relatively unexplored [14]. Organs and tissues such as the eyes, blood vessels, and gastrointestinal tract can pose unique challenges for the implementation of MNs for drug delivery; their varied structural (physical) and environmental (dynamic) properties require MNs tailored for the implantation sites. Successful utilization of MNs for non-transdermal applications requires structural flexibility and facile surgical use to suit the curved and complex surfaces of native tissue. Moreover, MNs should be able to penetrate soft target tissues within the body that may not possess the mechanical properties to sustain high application pressure.

In this review, we examine recent studies employing MNs for the delivery of therapeutics across different biological barriers, excluding transdermal applications, which have been

extensively discussed by previous reviews [15-18]. The evolution of MN development including fabrication techniques, material selection, and applications are reviewed and discussed. Additionally, state-of-the-art applications for non-transdermal drug delivery using MNs are described in detail. The current status of MN technology, in terms of commercialization and a perspective on future research directions, is also highlighted.

2. Microneedle fabrication

Currently, there are four main types of MNs used for drug delivery: solid, hollow, drug-coated, and dissolvable or biodegradable MNs (Fig. 1). Solid MNs are typically used in dermatology [19] as a pretreatment to form micro-incisions which allow a drug formulation to be administered with high permeability across the tissue barrier (Fig. 1A). In this approach, drugs are mixed with polymeric coating formulations and coated onto the surface of MNs for localized drug delivery [20-22] (Fig. 1B). In another approach, dissolvable or biodegradable MNs are used for sustained drug delivery as they harness biofunctional materials to maintain drug stability in MN patches (Fig. 1C). Also, hollow MNs are used to provide defined channels for targeting therapy to specific tissues [23-25] (Fig. 1D). Traditionally microfabrication and micromachining techniques have been utilized to create different types of MNs. More recently other fabrication methods such as drawing lithography and advanced molding technology have also been used to make MNs with different shapes (aspect ratio = 0.7–100) and sizes (height of 200–2000 μm).

2.1. Microfabrication

Microfabrication technologies adapted from manufacturing integrated circuits have proven to be well suited for the mass production of MNs with high reproducibility. The first MNs were developed from silicon where conventional microfabrication techniques, including photolithography, thin film deposition, and etching were used for their fabrication [5]. The final MN shape and dimensions depend strongly on the final fabrication step, which is either a wet etch or a dry etch process.

The versatility of the dry etching process allows the creation of MNs with more diverse shapes and dimensions. Dry etching allows the user to control process parameters including the gas flow rates, etch pressure, temperature, power and bias, and type of masking layer. The factors can be changed on demand to tailor the shape of MN for the desired application. Alternatively, wet etching has limited outcome in terms of MN shape. The first silicon MN (Fig. 2A) produced for drug delivery was fabricated by deep reactive ion etching (DRIE) of silicon wafers [5,26]. A 20×20 MN array with needles 150 μm in height and 150 μm spacing was generated on a 2 cm $\times$ 2 cm chip. Conventional silicon dry etchants such as SF_6 and O_2 were used to etch the silicon in the vertical direction, whereas CF_4 was used to prevent lateral undercutting (Bosch process) resulting in high aspect ratio (AR) MNs. The Bosch process was used to define the length of the MN. The initial passivation step provided an extra protection to the tip of MN. For example, a MN tip with a height of 40 μm and an AR of 1 was formed by excessive underetch using O_2 and SF_6 [27]. Subsequently, utilizing the Bosch process, the group was able to obtain MNs with an AR of 3. Several groups reported 150 μm tall MNs which were 45–50 μm in diameters at the base (AR = 3) [28] Fig.

2B), 250–300 μm tall MNs with 80 μm diameter (AR = 3–4) [29] and 320 μm tall MNs with 10–50 μm diameters (AR < 32) [30]. Moreover, the Bosch process was also used to make a hole in tapered hollow MNs [31-33] (Fig. 2C).

Silicon MNs were also made using an anisotropic wet etch processes. During the wet etch process, the etch rate depends on silicon crystal plane orientation, unlike dry etching in which the etch rate is independent of crystal planes [5,26-33]. A square-patterned mask was used with wet etching in potassium hydroxide (KOH) solution to produce both master and mold MN parts with lower fabrication costs. A (100) wafer with a square mask pattern can be etched by KOH solution to make pyramidal MN cavities, tapered at 54.72° [34,35] (Fig. 2D). Embossed MNs can be fabricated in various shapes by changing the chemical etchant, bath temperature, or mask design. MNs with an AR of 1–1.15 and height of 70–80 μm were molded from a single silicon wafer and employed for DNA injection into plant and animal tissues [36]. To make the master mold, a (100) silicon wafer and patterned mask array were placed in a KOH solution and the wafer was etched. The shape of the master mold MN depended on the concentration (29%) and temperature (79 °C) of the KOH solution and the shape and dimension of the mask array (Fig. 2E). MNs with an AR of 1.5 were fabricated reproducibly and the height of MNs was proportional to the size of the square mask [37,38]. In addition, the density of MNs in an array can be increased by up to 50% by changing the mask shape to be a square, circle, or diamond. Adding etch compensation structures such as a squares with fingers (primary square with squares at corners or squares with beams) can also alter the shape and density of the MN [39]. A combination of KOH etching and dicing has been adopted to make more complex MN structures to improve their insertion ability [40]. Dicing between the mask patterns can adjust KOH etching properties, helping to fabricate different types of MNs (Fig. 2F).

2.2. Other techniques

Several attempts have been made to fabricate MNs using conventional laser ablation and cutting. For instance, pyramidal MNs were fabricated by direct laser ablation of metallic materials using excimer lasers which can be used to obtain sub-micron resolution [41] (Fig. 2G). 40 μm long MNs were shaped by modifying manufacturing parameters such as the number of laser shots and the AR of the apertures in the mask. Another study also used laser ablation for MN fabrication from a metal sheet [42]. The group demonstrated the ability to form MNs with heights >10 μm and tip diameters <0.3 μm in the form of 5×6 arrays. Planar MNs were produced by cutting metal sheets using an infrared laser. The two-dimensional (2D) MNs were cut into the stainless steel plane and then bent at 90° out of the plane for the MN array [20] (Fig. 2H).

SU-8 photoresist has been used extensively to develop MNs. Two layers of SU-8 solution were spread on Pyrex glass to form a bilayer. The second layer of SU-8 was exposed to UV through the backside of the glass plane. By doing so, a tapered SU-8 pillar array, with tapered angles of 3.1°~5°, was formed on top of the SU-8 layer. The resulting 10×10 MN arrays was able to produce MN heights of both 200 and 400 μm [43]. MN structures with sharp tips were formed using combinations of tapered SU-8 pillars on a glass substrate as microlenses to taper the UV light path through this SU-8 pillar [44] (Fig. 2I). A

hemispherical cavity array was etched into a glass substrate covered with a chromium mask. Integrated lenses with a patterned layer of SU-8 facilitated the refractive index mismatch of the cavities filled with SU-8 in the glass substrate. The focal length and light path could be adjusted by varying the opening size and diameter of the lens, which was capable of fabricating MNs of various sizes. 200 MNs (4–6 AR, 400–1500 μm length) were fabricated with a single step of UV exposure in this system.

Three-dimensional (3D) printing has recently been used to produce MNs as well. Although 3D printing is a fast and cost-effective fabrication process, an additional process to elevate the printing resolution is usually adopted to obtain MNs with sharp tips. Luzuriaga et al. fabricated MNs through fused deposition modeling (FDM) 3D printing of poly (lactic acid) (PLA) [45]. To precisely define the tip of the MNs, they first printed a pillar array (200–2500 μm in height and 400–600 μm in diameter) and then etched the printed array in 5 M of KOH solution for 9 h. The etched MN array maintained their original length, while their diameter and tip size were decreased (200–300 μm and 1–55 μm, respectively). Stereolithography (STL), which has higher resolution than FDM, has been often used alone to print polymeric MN patches for transdermal insulin delivery as well [46] (Fig. 2J). However, the height and diameter of the printed MNs were around 1000 μm and the resolution was still lower than that of MNs produced with conventional fabrication techniques. Shrinkable hydrogels can be an alternative to enhance the resolution by using them as a MN mold material [47]. Hydrogel MN cavities were molded with STL-printed MNs. This hydrogel mold was subsequently dehydrated, reducing the size by up to 40%. Polyvinyl pyrrolidone (PVP) was cast in the shrunken mold, resulting in MNs with 9.6 μm tip diameters.

2.3. Drawing lithography

Though etching has been the predominant method for the fabrication of MNs, this technique faces critical challenges and is limited by its fundamental subtractive nature. Drawing lithography, however, has emerged as an alternative method to develop 3D polymer structures directly from a 2D film surface. Thus, drawing lithography boasts superior speed and cost-efficiency, achieving rapid prototyping of MNs for advanced biomedical applications compared to other fabrication techniques.

The first drawing process for MNs was developed with SU-8 and precisely machined stainless micropillars [48] (Fig. 3A). In this approach, a spin-coated SU-8 substrate was drawn by the micropillars and cured to solidify the polymeric bridge. The MNs were subsequently formed by increasing the drawing speed to 700 μm/s. Nickel electroplating was carried out for metallization of the surface of the drawn MNs and then the hollow metallic MN array was released by elimination of the drawn SU-8 MNs, using SU-8 remover. Although this technique can be used to fabricate ultra-high AR (over 100) MN arrays, the process was time consuming (1—2 h) and was unable to control the MN body profile. A similar process can be used to provide shape control, spatiallydiscrete thermal drawing can be used to achieve specific body profiles for MNs. The system consists of two heating elements controlling the temperature of both the substrate and drawing pillar, integrated with a micro z-axis stage [49] (Fig. 3B). This drawing method led to the fabrication of

biodegradable MNs with ultra-sharp tips while also providing control over the shape of the MNs. The shape produced is a function of the spatial control of the drawn polymer temperature, as well as the drawing steps and speed. For example, by adjusting the viscosity and surface tension of a drawn polymer, MNs with ARs of 1.5 to 7.0 were fabricated [50,51]. In one study, rapid fabrication of MN arrays by drawing lithography was performed with a UV curable resin [52]. MNs with different heights and ARs were produced by modulating the viscosity of the resin and the heat applied. MNs having an AR of 0.7–1 and hundreds of micrometers in height were fabricated in under 10 min.

Several types of drawing lithography have been developed to produce a variety of MN arrays. Another example of this methods versatility is its ability to draw a drug-containing polymer without heating for direct MN fabrication. Droplet-born air blowing-based drawing lithography has been developed to fabricate MNs containing biological drugs, without any molding process [53] Fig. 3C). Polymer solutions were dispensed onto both lower and upper plates. The droplet arrays were brought into contact and drawn at a rate of 5 mm/min. Air was blown at room temperature to solidify the drawn polymer. This droplet-born air blowing process provides fabrication conditions compatible with biological agents due to avoiding heat and UV exposure. In this study, 6×9 arrays of 600 μm-height MNs bearing insulin were produced within 10 min.

Furthermore, non-contact-based drawing lithography techniques have been developed using electromagnetic [54,55] or centrifugal forces [56]. Electro-drawing methods were introduced to rapidly fabricate biodegradable MNs [54] Fig. 3D). In this approach, an electric field was applied across the upper and lower sides of droplets at room temperature and, subsequently, MNs with heights ranging from 200 to 800 μm were formed in a single step. This contact-free method is mold-free and is suitable for producing polymer MNs, that are vulnerable to heat and mechanical stimulation. Another electro-drawing technique is magnetorheological drawing lithography [55] in which a MN can be drawn from a liquid droplet of curable magnetorheological agent by applying external magnetic fields. Two key factors for forming liquid MNs, elasto-capillary self-thinning and magneto-capillary self-shrinking, were investigated. The volume of the droplet and external field intensity were the important parameters used to control the MN height and tip sharpness. Finally, centrifugal lithography has also been developed for the production of MNs encapsulating biopharmaceutics [56] (Fig. 3E). This method is composed of a single centrifugations step in which a sessile drop of viscous polymer solution is placed on a surface. The major advantage of this method is the simplicity, as it does not require complicated precise mechanical parts. MN arrays with heights ranging from 200–1000 μm could be formed with 0.4–1 mg of polymer drop under 450 g of centrifugal acceleration. The material used in this study solidified as the solvent evaporated quickly at room temperature during the centrifugation step; no additional processes such as UV irradiation, heat, or forced air were needed.

2.4. Advanced molding techniques

Due to the complexity of the manufacturing processes described above, MNs are frequently used to create additional molds by application to casting substrates. The creation of molds from primary MNs facilitates cost-effective production and the ability to trial materials

incompatible with conventional microfabrication. After the primary MNs are molded by polydimethylsiloxane (PDMS), the MN cavities are filled with polymers, biological drugs, mixtures of polymeric carriers, or novel functional materials. Various materials, including carboxymethyl cellulose (CMC) [57,58], PVP [59,60], polyvinyl alcohol (PVA) [61,62], and sugars [63-65], have been dissolved in water and cast into molds created from primary MNs to fabricate dissolving MNs. Hydrogels, many of which are biodegradable, have been used for fabricating dissolvable MNs, enabling control over drug release by adjusting the degree of hydrogel crosslinking [66,67].

Biodegradable poly(lactic-*co*-glycolic) acid (PLGA), which is used in FDA-approved products, has also been used [68,69] to yield stronger and stiffer mechanical properties compared to other biodegradable polymers. Silk fibroin has recently emerged as a candidate for biomedical applications because of its superior biostability and mechanical properties [70]. Silk fibroin MN arrays have been developed by using methanol treatment to tune the degree of crystallinity, thus modulating the resulting drug release profile from MNs [71] (Fig. 4A). Biodegradable polymers have also allowed the creation of swellable MNs that can mechanically interlock with tissue, serving as an alternative to sutures [72]. These MNs consist of block copolymers, with swellable polystyrene/polyacrylic acid tips and a non-swellable polystyrene core. The conical MNs were inserted into the skin with minimal insertion force and sufficient depth, while still maintaining high adhesion strength in the hydrated, swollen state (Fig. 4B). Other swellable MNs have also been reported. One system created needles from UV crosslinkable methacrylated hyaluronic acid (HA). This hydrogel-based MN had high water affinity, allowing for the rapid uptake of interstitial fluid; this fluid collection did not require an additional device and facilitated the metabolic analysis of the withdrawn fluid [73].

The solidification of polymeric solution or melt enables MNs to stay fixed to a macro-scale structure. Separable arrowhead MNs that can deliver vaccines and drugs to the skin were developed through multiple molding processes [60]. The MNs were fabricated by casting arrowheads, encapsulating therapeutic agents, into a mold. The arrowheads were subsequently fixed to arrays of metal shafts to form the macro-scale structure for use (Fig. 4C). Another sharp tip-separable MN device was also developed, utilizing a silicon support array [74]. Chen et al. also developed similar separable MN patch consisting of upper chitosan MNs and a supporting PLA array. Chitosan MNs were fixed to the top of a PLA array, which provided sufficient mechanical strength for the MNs to be fully inserted into the skin [75]. Lee et al. fabricated biodegradable PLGA MN arrays on a flexible PLGA surgical meshes [38]. MNs were molded and integrated with a medical mesh by thermal welding on a 3-axis microstage (Fig. 4D). MN cavities were arrayed on a PDMS mold and each cavity was individually filled with molten PLGA. An adhesion layer was left above the plane of the PDMS to facilitate the attachment of the needle to the mesh. Once the PLGA mesh was laid on the filled PDMS mold, a heated micropillar was used to melt the adhesion layer above each needle, thus fixing the cast needle to the mesh upon cooling.

Material crosslinking can also be used to adapt MNs for integration with macro-applicators for more effective clinical use [76]. Transfer molding methods have been used for MN fabrication for ocular tissue applications, in which it is difficult to inject MNs manually.

Song et al. published a study regarding the design of an applicator for corneal stromal injection of biodegradable drug-loaded MNs (Fig. 4E) [77]. The group fabricated a PDMS mold by chemical wet etching with KOH solution as previously mentioned [34,35]. Each MN cavity was filled with SU-8. A pen-like applicator used UV curing to crosslink the SU-8 MN on the tip of the pen. The MN attached to the pen was coated with drug formulations and applied to mouse corneas. The MN pen could deliver drugs into the stromal cornea with minimally invasive incisions and without perforation, demonstrating that the MN pen could both create and deliver MN for safe, localized drug delivery. Park et al. also developed a similar pen-type MN injection system for scleral injections [78].

Beyond topical drug delivery with coated MNs, a transfer molding technique was developed to create hybrid-material MNs and attach them to a pen applicator in a single step [79] (Fig. 4F). This hybrid MN pen assembly consists of a tip composed of drug-loaded PLGA and a MN base made of SU-8. To achieve this, a 150 μm length, 1.5 AR, and octagonal cone-shaped MN was microfabricated by wet etching and a complementary PDMS MN cavity was subsequently molded. The drug-PLGA material was added to partially fill the mold cavity (premolding). Pressure-assisted transfer molding was performed next by pressing an SU-8 droplet transferred to an applicator tip above the pre-molded drug-PLGA material. UV curing led to the formation of a multi-layer detachable hybrid MN at the tip of the applicator. In clinical use, the pen was used to deliver the MN into the ocular tissue, only detaching the drug-loaded tip into the tissue as the SU-8 MN base retracted into the pen. This left the PLGA tip within the tissue for sustained and local drug release.

3. Materials for implantable microneedles

For the fabrication of non-transdermal, implantable MNs, material choice is critical. Initially, silicon MNs fabricated on wafers by microfabrication were used due to their high mechanical strength, allowing MNs to pierce skin [5] and brain tissues [80,81]. However, the in vivo applications of silicon are limited due to its brittle nature [82,83]. Though Bayliss et al. demonstrated that nanocrystalline silicon does not have significant cytotoxicity [84], there are reports describing formation of granulomas [85]. Overall, the biocompatibility of silicon is still uncertain and the interaction of silicon MNs with native tissues should be further investigated. Parylene coating is one possible approach to improve biocompatibility; it is currently used as a coating for some commercial medical implants to limit the biological response. Parylene coating can be applied using vapor deposition to achieve uniform coating on implants, providing complex and fine surfaces. Hence, it is suitable for application to MNs. Studies have demonstrated improved long-term biocompatibility by coating parylene onto MNs that were subsequently inserted into the brain or skin [86,87]. Also, some metals have properties that are attractive for MNs, such as high mechanical strength. Among them, titanium alloys have shown good biocompatibility and corrosion resistance [88]. For these reasons, titanium MNs have been fabricated for transdermal delivery systems [89] and bio-sensors [90,91].

Carbohydrate-based materials have been extensively used in MNs for tissue insertion due to their excellent biocompatibility and degradability. Maltose is the most commonly used carbohydrate for MN array production [65] and has been frequently used in various

parenteral formulations approved by the FDA [92]. Also, trehalose, mannitol, sucrose, and xylitol have been used as cryoprotectants, stabilization agents, and nutrition products [93,94] which attests to their biodegradability for MN application [63]. Cellulose derivatives such as CMC have also been used to make degradable or coated MNs [57,77,95]. Chitosan and HA have both been widely used as raw materials for drug delivery carriers and cellular scaffolds [96]. An attractive characteristic of chitosan is its ability to be degraded by lysozymes through the hydrolysis of its acetylated residues; accordingly, MNs made of chitosan were successfully fabricated for vaccination delivery [75]. HA has been widely used for transdermal drug delivery systems, including MNs. HA and its derivatives have been developed for drug delivery applications due to their degradation by hyaluronidase found in the extracellular matrix after endocytosis [97]. Currently, HA MNs are being vigorously pursued for use in the cosmetic field [53,56].

Generally, a polymer's biocompatibility is dictated by its ability to limit the foreign body response. Synthetic polymers, such as polycarbonate (PC) and polymethyl methacrylate (PMMA), are effective at limiting this response and have been extensively used in the medical field [98,99]. Both have applications to MNs as PMMA has been used for the creation of MN master molds [100] and PC has been adopted by transdermal solid MN arrays coated with calcein gel [101]. SU-8 is an epoxy-based, photocrosslinkable polymer used widely for the fabrication of MNs as microelectrodes and has been used for measuring electrical impedance in bio-tissues [102], monitoring neural spikes [103], and for sensing intraocular pressure [104]. Nemani et al. demonstrated the ability of SU-8 to support cell viability *in vitro* and *in vivo* [105].

Biodegradable polymer MNs have been developed to completely dissolve in the skin, leaving no biohazardous sharp waste after use. PVP and PVA have been broadly used for biomedical applications due to their swelling properties and bioadhesivie characteristics [106,107]. In addition, PVP presents low cytotoxicity because of high water solubility [107,108]. PLA, PGA and PLGA are aliphatic polyesters and have been used extensively for drug delivery systems such as MN production [109]. These biodegradable MNs are degraded after penetrating the skin [69] and vascular tissue [51,110]. The degradation time of polyesters can be manipulated by varying the ratio between PLA and PGA in the copolymer of PLGA [109], which enables the control of drug release over time. Silk fibroin was also used to fabricate MNs using aqueousbased micromolding. The fabrication was carried out at room temperature for the bulk loading of MNs with drugs, including vaccines, peptides, antibiotics, or any temperature-sensitive therapeutics [70]. The controlled drug release profile of the MNs was demonstrated in one study in which the biodegradability of silk MNs was controlled by varying the contact time of methanol treatment [71].

4. Applications of implantable microneedles

Many organs in the body suffer from ineffective drug delivery approaches. This problem may be addressed by using MNs. However, unlike skin, other tissues or visceral organs in the body do not have sufficient posterior repulsive force against MN insertion. To effectively apply MNs to these tissues, additional surgical processes may be needed, or MNs should be fabricated to allow conformal contact to soft, poorly supported 3D curved tissues. To achieve

these goals, MNs can be combined with customized injection application devices for effective MN insertion. MNs can also be fabricated in the form of curved or flexible patches. This section explores emerging MN applications for non-transdermal drug delivery, which has been driven by the expansion of MN technology in recent years.

4.1. Ocular tissue

Serious illnesses can occur both in the front and back of the eye (Fig. 5) [111]. The eyeball can be divided into two segments in the context of drug delivery routes: (1) the anterior segment consisting of the iris, lens, cornea, trabecular meshwork, and aqueous humor in the anterior chamber, and (2) the posterior segment consisting of the sclera, choroid, retina, vitreous humor, optic nerve, and macula. Diseases affecting the back of the eye, such as age-related macular degeneration, diabetic retinopathy, and uveitis are the leading causes of blindness in the world. The anatomical and physiological constraints of the eye make drug delivery to the posterior eye a major challenge. The cornea, where most of anterior segmental diseases occur, consists of five layers in the outermost part of the eye and is void of blood vessels [112]. Therefore, the cornea obtains its nutrients from the aqueous humor and tears. A tear film bathes the surface of the cornea and helps in protecting the eye from irritants. In general, the structure of corneal tissue, continuous fluid turnover, and eyelid blinking act as physical, static, and dynamic barriers around the anterior segment of the eye and pose major obstacles to drug delivery.

4.1.1.   Anterior segment—In the first trial of MN application to the front of the eye, laser-cut metal MNs coated with DNA and proteins as model drugs were inserted *ex vivo* and *in vivo* into the human cadaveric sclera and rabbit eye [22]. The results showed an enhanced efficiency in *in vivo* MN drug delivery. Moreover, the bioavailability of the eye was improved by 1 to 2 orders of magnitude comparing to topical eye drops. This demonstration of MN applicability inspired further ocular MN developments. With a similar MN platform, bevacizumab-coated MNs were applied to the cornea for treatment of corneal neovascularization [113] and demonstrated no observable adverse effects in clinical and microanatomical analyses. The major limitation of coated ocular MNs is their restricted loading capacity, which inhibits their widespread adoption for large-scale and clinical applications. To maximize the drug coating capacity of planar MNs, DRIE was used to fabricate 2D MNs with complex fenestrations as drug loading reservoirs [114] (Fig. 6A). Fenestrated MNs increased drug loading efficiency up to 500% compared to solid MNs (without fenestration). The drug delivery efficiency was evaluated using spectrophotometry and fluorescence microscopy in an *ex vivo* rabbit corneal tissue.

Beyond coated MNs, dissolvable MNs have been developed for posterior segment drug delivery. For example, Raghu et al. fabricated a PVP based 3×3 MN array in a conical shape with 800 μm height and 300 μm base width *via* conventional molding process [115]. The release profile of PVP (M_w = 70 and 150 kDa) was controlled by varying its molecular weight. The dissolving MN contained 0.96–9.91 μg of drug and released the drugs within 10–180 s. An *ex vivo* drug permeability test with porcine eyes demonstrated that the PVP-based MN array was able to deliver the drugs with higher permeability than eye drops. Another approach using the same dissolving MN platform delivered besifloxacin to the

corneal tissue [116] (Fig. 6B). The 6×6 dissolvable MN array contained around 100 μg of besifloxacin, which targeted delivery to the human cornea. Patching MNs for 5 min significantly improved the drug permeation and distribution in the cornea, showing greater antibacterial activity in an infected cornea in comparison to free besifloxacin solution. Than et al. introduced a detachable MN array as an eye patch [117]. These MNs could be inserted into the cornea and provided MN reservoirs with controlled release by harnessing two different materials (HA and methacrylated HA) for MN molding. The kinetics of biphasic drug release enhanced its therapeutic efficacy. They showed that the MN patch loaded with an anti-angiogenic monoclonal antibody reduced ~90% of neovascular area in the cornea of neovascularized mouse models.

A prerequisite for successful corneal drug delivery with MNs is insertion into the cornea, without penetrating the entire depth of the corneal tissue. However, this is difficult to as the cornea is thin and structurally inadequate while the aqueous humor supporting the cornea from the back does not generate large enough repulsive forces to insert MNs. For situations like these, MN insertion has been performed by combining a MN with an injection assisting applicator [77,79]. One solution is a spring-loaded pen platform which was used to inject MNs instantaneously using a spring-generated impact. As a result, MN insertion into the cornea became facile and independent of the weak mechanical properties of the tissue. In the first attempt, the MN was assembled to the tip of pen and applied to the mouse cornea [77] (Fig. 6C). To do that, the SU-8 MNs were integrated with a customized pen applicator by transfer molding technique with the PDMS mold as described earlier in Section 2.4. The MN pen was able to deliver rhodamine B into the stromal cornea with a minimally invasive incision and without major perforation compared to syringes and 30 G needle tips. Moreover, the efficacy of the MN pen coated with sunitinib malate was demonstrated for treating neovascularization in a corneal angiogenesis model (Fig. 6C).

The above ocular drug delivery MN systems for the anterior segment of the eye can be adapted for sustained drug delivery for the treatment of infectious diseases, such as keratitis. Repeatable topical eye drops often fail to heal keratitis due to poor patient compliance. Drug eluting contact lenses, which enable sustained drug release, also suffer from side effects induced by the block of corneal oxygen transportation. For this reason, there is a need for a drug administration systems that require minimal and infrequent application and a minimal drugreleasing matrix. Novel detachable hybrid MN pens (d-MNPs) with biodegradable tips containing drugs have been developed using a transfer molding technique for corneal stromal injection [79] (Fig. 6D). For successful corneal injection of a 48 μm height drug-tip, MN injection dwell time (10 s), MN spring load (k = 2.29 N/mm), and MN insertion depth (86 pm) were optimized using mechanical compression and *in vivi* testing. After injection under this condition, only the drug-loaded tip of the MN detached from the pen applicator and stayed within the tissue to gradually release the drug for up to 7 days. Therapeutic efficacy of the d-MNP was also demonstrated using a mouse acanthamoeba keratitis model. When compared to the control sample, there was no decomposition or side effects caused by d-MNP injection in the diseased cornea 1-day post injection. Four days post injection, the opacity of cornea was reduced in the d-MNP treated sample. This therapeutic effect continued to be observed for the following two days (Fig. 6D).

4.1.2.   Posterior segment—Diseases associated with the posterior segment of the eye require drugs to reach the macular or peripheral retina. Conventional drug delivery has been achieved by intravitreal injection, which is directly injected through both the sclera and the vitreous humor. Although this method can deliver drugs reliably, it is invasive because it penetrates into all tissues and can cause intraocular infections [118].

Hollow MNs were successful at depositing drugs into the narrow space between the sclera and the choroid called the suprachoroidal space (SCS) [119], instead of intravitreal injection (Fig. 6E). In this work, MNs were inserted into the human sclera 5–7 mm from the limbus. A pen-like injection device integrated with the hollow MN was able to control the extrusion length of MN from 700–1000 μm. Injecting drugs in this manner enabled sustained drug delivery from the SCS and reduced dosing frequency. Targeting the SCS route led to increased concentrations of drugs in the posterior segment than in the anterior segment (up to 10-fold), while intravitreal injection had no selectivity between the posterior and anterior segments. Since the resistance to flow in expandable SCS was much lower than through the relatively incompressible surrounding tissues, the MNs did not need to physically enter the SCS or open it by blunt dissection. The fluid injected by the hollow MN naturally flowed into the SCS in a few seconds and expanded it anatomically. In another study, a formulation was developed in which a drug model penetrated the SCS layers and was delivered to the back of the eye during the SCS injection with a MN [120]. Furthermore, the effects of formulation composition, injection volume, and time on circumferentially spreading drugs were characterized after applying the MNs to rabbit eyes [121]. Such MN injection into the SCS has been clinically validated by Clearside Biomedical (Alpharetta, GA). They have performed several clinical trials for the commercialization of a MN injector for drug delivery through the SCS (US Clinical Trial NCT02952001).

A MN pen, similar to the previous study for the anterior segment drug delivery, was adopted to deliver drugs to the posterior segment [78] (Fig. 6F). In the latter study, Park et al. developed a system that was easy to use and enabled impact insertion. By using the device, the insertion speed was controlled. It was expected that the model drug, or small molecule, could be delivered effectively in the sclera by controlling the wound depth of tissue. To control the insertion depth based on the insertion speeds, three types of springs were used. The spring constants of the springs were 73.5 ± 5.1, 360.2 ± 10.3, and 1561.4 ± 10.4 N/m, respectively, and the insertion depths were 58, 219, and 312 μm, respectively. Diffusion of rhodamine B through the sclera was compared among three different groups: 1) topical administration; 2) manually-inserted MN; 3) MN pen insertion. The *ex vivo* tests showed that the sclera treated by the MNP had the most concentrated and largest area of distribution of rhodamine B. The *in vivo* results using beagle eyes confirmed that rhodamine B diffused throughout the sclera from the insertion site in the limbus to the back of the eye.

Thin hollow MNs may be used for general intravitreal injection but should be long enough to pierce the outer barrier of the eye, without mechanical failure of the MN against robust sclera tissue. This is a challenging issue for MN application to the outer barrier of the eye. To achieve this, ultra-high AR and hollow MNs (called tower MN) have been fabricated by reverse drawing lithography on blunt conventional needles [122] (Fig. 6G). A beveled MN tip with 15° angle to the tower MN was fabricated using laser cutter to achieve an alternative

intravitreal injection with minimal invasiveness. Sympathomimetic phenylephrine solution was administered into the vitreous humor of rabbit eye by the tower MN and an effective intravitreal delivery was demonstrated through pupil dilation measurements (Fig. 5).

4.2. Vascular tissue

Arteries and veins have three layers: the adventitia is the outermost layer consisting of loose connective tissue, it serves as a protective layer, and prevents overstretching; the tunica media is the middle layer composed of smooth muscle cells and functions in dilation and constriction of the blood vessel; and the tunica interna, the innermost layer, is composed of endothelium (Fig. 7). One of the main components of vascular diseases is narrowing of blood vessels, caused by atherosclerosis. Atherosclerosis, which occurs due to the buildup of plaque in the walls of the arteries, makes blood flow sluggish in the vessel. If a blood clot forms, it can completely occlude blood flow and result in a myocardial infarction or stroke. The narrowing of blood vessels develops in different forms according to extensive pathological causality, but in the early stage of pathogenesis, neointimal hyperplasia occurs due to the abnormal prolific growth of smooth muscle cells in the tunica media layer [123,124]. Perivascular (*via* the outermost layer) and endovascular (*via* the innermost layer) can be a route for drug delivery with some impediments, owing to the microscale thickness of the adventitia and endothelium, which act as physical barriers. To overcome these hurdles, advanced MNs have been developed for facile drug delivery using perivascular and catheter-based endovascular devices.

4.2.1. Perivascular—Several perivascular drug delivery devices have been developed including ethylene-vinyl acetate wraps with paclitaxel [125], polycaprolactone (PCL) and PLGA wraps [126,127], and sirolimus-eluting collagen membrane [128]. However, non-biodegradable devices, such as ethylene-vinyl acetate wraps, have issues with device removal once the drug has been delivered. Other biodegradable wraps such as PCL and PLGA do not have the removal problem, however, passive drug diffusion, from the wrap to the vascular tissue, reduces drug delivery efficiency. MNs are a potential remedy to the delivery efficiency challenge as they have been demonstrated to achieve high efficiency percutaneous drug delivery. The first perivascular MN application was developed as a cuff shape, which enabled the MN array to make conformal contact with a curved perivascular surface [110]. The 3×3 PLGA90/10 MN array was fabricated *via* the thermal drawing process mentioned earlier [49]. The MN array was coated with a drug formulation, mixed with PLGA50/50, and curved by a post-annealing process (MN cuff). The MN cuffs were applied to the rabbit abdominal aorta *in vivo* to test the efficacy at treating neointimal hyperplasia (Fig. 8A) [51]. By implementing the thermal drawing process, optimal height (650 μm) and AR (3.5) of the MNs for effective penetration into rabbit vascular tissues was demonstrated *in vivo.* Dip-coated MNs with PLGA drug formulation were shown to release up to 1 μg of drug for 2 weeks by PLGA degradation [49]. The drug coated MN tip could reach tunica media without puncturing the vessel. Subsequently, concentrated drug distribution within only the middle layer of the aorta was confirmed (Fig. 8A). Upon comparing the *in vivo* drug delivery of the MN cuff and non-MN cuff (film), the delivery efficiency of cuff was about 200 times higher than that of the film (Fig. 8A). *In vivo* tests were performed with a balloon injured rabbit model with induced neointimal hyperplasia. As

a result, neointimal hyperplasia formations in tissue treated with MN cuffs were reduced from 28% to 11% relative to an untreated control group (Fig. 8A). To scale up the MN cuff for potential clinical translation, various drugs, such as sirolimus and sunitinib, other than paclitaxel were used to confirm the therapeutic effect and safety [129].

Lee et al. developed a perivascular flexible PLGA MN mesh as an upgraded version of the MN cuff that can be gently installed on the blood vessels with minimal mechanical rigidity [38] Fig. 8B). A transfer molded PLGA MN array on flexible PLGA surgical mesh was dip-coated with drugs. To understand the feasibility of this MN mesh for vascular drug delivery, an *ex vivo* insertion test was performed using rabbit aorta and prepared for histopathological analysis to confirm MN insertion appearance. *In vivo* animal studies were demonstrated in rabbits, with 2 and 4 week follow-ups to prove the safety and effective drug delivery of the MN mesh. After follow-ups, all treated blood vessels were collected and prepared for histopathological analysis. Finally, they discovered MN insertion into the tunica adventitia enhanced drug distribution into the tunica media in addition to improving the structural stability of blood vessels with an applied MN mesh.

4.2.2. Endovascular—In endovascular drug delivery, the Bullfrog® and Cricket® Microinfusion devices from Mercator Medsystems Inc. (Emeryville, CA, USA) have been introduced by combining a 34G micro-scale needle with a balloon catheter [130,131] (Fig. 7). Physicians can position the Bullfrog® catheter in the peripheral artery or the Cricket® catheter in the coronary artery using standard interventional procedures. While the catheter is closed, the MN is covered by the balloon, as to not injure the vessel walls. When the catheter is opened, the MN comes out of the balloon to inject drugs directly to the surrounding luminal tissue. Subsequently, the drugs are deposited and will diffuse inward through the vessel layers (Fig. 7). The puncture by hollow MNs is insignificant and in most cases seals immediately without bleeding. Owens et al. reported the utilization of this catheter for the delivery drugs [130]. This was the first trial in humans to test the safety and feasibility of dexamethasone administration to the superficial femoral and popliteal artery with a Bullfrog® catheter. Results showed that there were no side effects related to the device. The dose and concentration of drug were adjusted to coincide with the length of the artery treated, contrary to passive elution from a fixed-length stent or balloon surface. Anti-inflammatory or anti-proliferative compounds were delivered into the adventitia of the vessel at the time of treatment to prevent restenosis following endovascular treatment. Sirolimus has also been delivered *via* MN to the femoral arteries in swine to prevent from restenosis [131]. No adverse events, signs of toxicity, mural injury, or evidence of thrombosis were observed following drug administration *via* the Bullfrog® catheter. In the treated vessels, sirolimus concentration decreased from one hour (8440 ± 6956 ng/g) to 72 h (624 ± 398 ng/g) and decreased through day 28 (122 ± 73 ng/g).

There is an additional study in which a microgroove of a similar structure, but not a MN, was applied to a drug eluting balloon (DEB). Balloon angioplasty with DEBs have emerged to treat stenosis, neointimal formation or in-stent restenosis by delivering drug into an endovascular lesion. However, DEBs still have limited delivery efficiency. Loss of drug by blood flow, when performing balloon angioplasty, results in low drug delivery efficiency of DEBs and contributes to systemic side effects. In addition, the drug delivery mechanism of

DEBs, especially related to contact pressure, has been sparsely investigated. For these reasons, Lee et al. developed a linearlymicropatterned drug eluting balloon (LMDEB), using a customized balloon forming machine and balloon forming mold [132] (Fig. 8C). LMDEBs were fabricated to have 16 linear micropatterns (LMs) with a feature height of 130 μm on the surface (Fig. 7). LMs can increase the contact force between the drug coated surface and lumen, which leads to the enhanced efficiency of endovascular drug delivery. A drug stamping test and mechanical simulation study confirmed this hypothesis. In addition, the amount of drug residue of LMDEB groups was 2.3 times higher than DEB groups after *in vivo* study and LC/MS analysis. Finally, they performed *in vivo* tests comparing the efficacy of LMDEB and DEB using atherosclerotic and in-stent restenosis models for 4 weeks. All of the major indicators of vascular disease, such as degrees of plaque formation, diameter stenosis, and area stenosis, were reduced in the LMDEB groups, compared to conventional DEB groups, with statistical significance ($p < .05$).

4.3. Other applications

4.3.1. Gastrointestinal tract

Gastrointestinal tract—Oral administration remains the most common method of drug delivery. However, poor drug absorption and drug degradation are major limitations with this delivery route. These obstacles are particularly challenging when introducing biologic drugs, such as insulin, which are susceptible to destruction by the extreme pH in the gastrointestinal tract. For this reason, a MN-integrated pill device was introduced [133] (Fig. 9A). The device was fabricated from acrylic 25G needles, protruding 5 mm from the surface, that were manually placed into the orifice, which was 2 cm in length and 1 cm in diameter. They demonstrated that MN-based delivery improved bioavailability of insulin in a swine model. They also showed that the MN devices could be passed and excreted from the gastrointestinal tract safely. These findings strongly demonstrate that MN technology can overcome the current limitations associated with drug delivery in the gastrointestinal tract.

4.3.2. Oral cavity

Oral cavity—While intratumoral injection of anti-proliferative drugs can be used to treat oral carcinomas, conventional hypodermic injections suffer from poor distribution and low retention in the tumor/systemic circulation while also causing pain to the patient. Doxorubicin (DOX) encapsulated by PLGA nanoparticles was prepared and coated on MNs, which were fabricated by a wet etching process from stainless-steel sheets (50 μm-thick) for minimal invasive intratumoral injection [134] (Fig. 9B). The MN array was applied to the cancerous region in oral phantom tissue followed by DOX delivery to a depth of 3 mm and lateral breadth of 1–2 mm. In addition, DOX diffused in porcine cadaver tissue up to a depth of about 4 mm and laterally in an area measuring 1 cm × 1 cm. Intratumoral injection with conventional hypodermic needles causes leakage of the drug delivered, however, the MN array demonstrated in this study shows the potential to locally administer the drug with uniform distribution within the tissue. Another challenge with oral delivery is saliva. Saliva contributes to low drug delivery efficiency by coated-MNs increasing fluid flux across the tissue [135,136]. To overcome this challenge, MNs were coated with a model drug sulforhodamine and inserted in to porcine buccal mucosa *in vitro* [137]. Permeation experiments were conducted for simulated dynamic and static salivary flow by adding phosphate buffered saline in the donor compartment of Franz diffusion cells containing

buccal tissue with inserted MNs. The results showed that sulforhodamine remained in the tissue after 1 day, despite the presence and flow of PBS on top of the MN insertion site.

4.3.3. Genitourinary system—MNs integrated with catheters, similar to the Bullfrog® discussed in Section 4.2.2, have also been introduced for periluminal drug delivery to genitourinary tissue [138]. This device can be targeted to the lesion and the MNs can be inserted to the wall of the luminal lesion. Until the MN was at the infusion site, it was positioned in an atraumatic configuration to prevent scraping against the wall of the lumen by any tip of the MN. Since the MN was hidden by the surrounding wall of a sheath, it would not injure the tissue when the physician was handling the catheter during intervention. When the MN catheter reached the injection site, the balloon was expanded to insert the MN to the central axis of a lumen. After MN insertion and drug infusion to the lesion, the therapeutic formulation was exhausted from the open area of the balloon and the balloon was retracted.

MNs integrated with the balloon can be used for treating a functional disorder of the urinary bladder in which the drug is delivered into the urinary bladder trigone through the vaginal wall [139]. This device included a MN array onto a triangular surface, corresponding to the shape of the trigone. The MN array was connected to a reservoir containing the therapeutic compound in fluid form. When pressure was applied to the reservoir, the fluid was expelled through the MN array into the vaginal wall. The reservoir was directly connected to the MN array and separated by a barrier that retains the drug in the reservoir until pressure is applied. Application of pressure breaches the barrier and forces fluid, containing the compound, out of the reservoir and through the needles in the array.

Drug delivery to the vaginal cavity is a suitable application for inoculation of mucosal vaccines because of its large surface area and mild environment, facilitating convenient administration and less safety concerns relative to other mucosal sites. Ning et al. developed dissolving MNs consisting of sucrose, PVP, and CMC for stably-loaded proteinbased vaccine agents [140] (Fig. 9C). They molded the MN array with a ready-made PDMS MN cavity and applied this device to mice. By delivering the vaccine adjuvant *via* a MN patch, they demonstrated effective vaccination in vaginal tissue, in terms of both antigen stability and administrative safety without side effects. These results have the potential to be translated into the clinic for use in preventing infectious pathogens, particularly those that are sexually-transmitted.

4.3.4. Cardiac muscle for therapeutic cell delivery—Recently, Cheng, Gu and colleagues showed the application of MNs for heart regeneration [141] Fig. 9D). In this study, MN-integrated cardiac stromal cells (MN-CSCs) secreting heart regeneration factors were loaded into the back of a MN patch composed of PVA. CSCs delivered with this approach could extract nutrients from the heart and the MN patch facilitated the diffusion of regeneration factors into the myocardial infarction (MI) site. Communication between the CSCs and cardiomyocytes was confirmed in a microfluidic model. Furthermore, the authors demonstrated that MN-based cell delivery enhanced angiomyogenesis in a rat model and protected cardiac function in a porcine model, both with limited toxic side effects.

5. Translation perspective and outlook

In this review, the current progress related to the fabrication, materials, and applications of non-transdermal MNs is summarized (Table 1). MN arrays with large surface area can be fabricated with wet or dry etching using semiconductor technology and drawing lithography can be used to make a variety of shapes in a short time with low cost. In addition, non-thermal drawing lithography can be used to develop polymeric MNs containing biological drugs to improve drug efficacy by avoiding harsh manufacturing conditions. Additionally, it is possible to increase the usability of MNs by casting a variety of biocompatible, biodegradable, and functionalized polymers into negative MN molds. Furthermore, MNs can be integrated with injector systems for effective tissue insertion and optimal drug delivery. These systems include various approaches of MN delivery such as depositing portions of the MN structure. The development of such MN technology has been applied not only to the conventional percutaneous drug delivery field, but also to delivery therapeutics to the eyes, blood vessels, and other tissues. By designing systems specific to the target tissue, it is possible to achieve high efficiency drug delivery that outperforms traditional drug delivery methods. The primary factors influencing the drug delivery efficiency of MN technology are the targeted insertion of the MNs into the correct tissue and the behavior of the drug carrier releasing the therapeutic. Therefore, as described above so far, much of the development surrounding MN technology has been focused on MN fabrication, the development of various materials capable of releasing drugs, and applicator devices for facile, standardized MN insertion.

The maturation of MN technology has broadened the range of applications to various tissues and also promoted commercialization of percutaneous drug delivery. Commercial use of disposable MNs to replace intravascular and intramuscular injections in combination with existing conventional syringes has also been actively pursued. MicronJet 600™ of NanoPass Technologies Ltd., Debioject™ of Debiotech and AdminPen™ of NanoBiosciences are systems that can deliver drugs in a common syringe. MicronJet 600™ has a pyramidal 600 μm high hollow MNs made by a silicon etching process [142]. The MNs in Debioject™ are 350–900 μm in height [25] and AdminPen™ consists of a planar MNs with heights of 500–1400 μm [143]. The 3 M™ hollow microstructured transdermal system (hMTS) established a platform for the production of various polymeric MNs and can deliver approximately 0.5–2 ml of drug formulation [144,145]. Based on this, Panacea Pharmaceuticals Inc. is currently undergoing FDA Phase 1 clinical trials using an immune system drug using the 3 M™ hMTS platform. Bayer Healthcare has developed a pen-type MN injector that can automatically inject drugs, named BETACONNECT™. It can deliver the drug by adjusting the dose, ranging from 0.25–1 ml, and delivery depth, from 8–12 mm deep, using a smartphone application. This system was approved by the FDA in 2015. Soluvia™, from Becton Dickenson (BD), and the SCS (suprachoroidal space) microinjector, from Clearside Biomedical Inc., store the drug in the syringe in advance, making it more convenient for drug injection. Soluvia™, having 1.5 mm long 30G MN, is pre-filled with the drug and injected into the skin with a controlled spring repulsive force. The SCS microinjector is precisely machined to a length of 700–800 μm through laser machining and electrolytic

polishing of 33G stainless steel MN to pre-fill the drug reservoir and deliver it to the SCS of eye [146].

In addition, vaccination through the percutaneous route has been developed using a MN patch and clinical trials for commercialization are actively underway [3,17,147,148]. Micron Biomedical's MN patch was developed in a shape similar to BAND-AID®, which makes it easy for anyone to apply this patch to the skin, reducing the demand for medical professionals. Recent FDA phase 1 clinical trial results confirmed safety and effective immunity acquisition. According to Australian clinical studies, Vaxxas' Nanopatch™ demonstrated more efficient immunotherapy efficacy than conventional medication in rat studies, using up to one-millionth of the existing drug dose. Beyond the manual application of MN patches, various types of injection tools are used to increase the efficiency of MN patches. MicroCor® from Corium International Inc. uses a dissolvable MN to further enhance drug stability. Beyond vaccinations, MN patches are commercialized in the field of cosmetics, where clinical application is relatively simple compared to internal organs. Karatica Co., Ltd. has developed a MN patch that has a wrinkle-reducing effect and is applied around the eyes and tucked skin. This product, named I'm Fill Needle Patch, is a 400-HA MN array containing the drug acetylhexapeptide-8. Junmok International's Royal Skin is also a HA-based MN array, which can contain lactose to deliver drugs through the skin. RAPHAS Co., Ltd. has developed a variety of products, including Acropass, a patch developed for the treatment of acne and wrinkles, which has been largely successful due to its use of the droplet-born air blowing process [53]. Though non transdermal MNs will undoubtedly face more stringent manufacturing and regulatory requirements than their transdermal counterparts, the laboratory to market pathways that have already been established in the commercialization of transdermal MNs will provide an excellent framework for translation.

Besides the drug delivery field, bio-sensing, by extracting interstitial fluid (ISF), is an emerging application for MNs. ISF has been addressed for bio-sensing analytes, such as lactate or glucose [149-152]. Continuous glucose monitoring (CGM) is of great interest in the field of bio-sensing with promising clinical evidence that the frequency of hypoglycemic episodes and levels of HbA_{1c} can be reduced by effective CGM in Type 1 diabetes [153]. Glucose monitoring is a key factor to treat diabetes, especially for those who are dependent on insulin [154]. A MN patch enables the sensor to be in continuous contact with the skin, where the ISF exists [155]. The microscale height of the hollow MNs provides channels between the inner layer of skin and external area for ISF sampling. Additionally, the MNs do not puncture the dermis, minimizing any damage to blood vessels and nerves in the dermis layer. Notably, signal noise and contamination from sweat can be avoided during sensing as the MN is not located on the surface of the skin and provides high-fidelity samples from the deeper layers of the tissue [155]. Jina et al. developed and tested a MN-based CGM system [156] that could measure a glucose signal for 3 days. To increase the lifetime of the MN-based CGM, biofouling within the MN channel must be inhibited. Potential routes to mitigate this issue include optimizing the needle parameters to have desirable length, AR, angle, and tip sharpness, modifying the surface of the MNs with an anti-fouling agent, enhancing the biocompatibility of MNs, or matching the mechanical properties to those of the tissue.

The last two decades have yielded the fruitful development of MN technologies, from innovations in fabrication techniques and materials engineering, to translational efforts for different biomedical applications. Further advances in manufacturing technology, biomaterials, and legal regulation will facilitate the widespread adoption of MNs for a variety of biomedical applications. The ongoing development and commercialization of new MN products will play a large role in bringing minimally invasive methods to enhance human health and improve quality of life into mainstream medicine.

Acknowledgements

References

[1]. Marzulli FN, Barriers to skin penetration, J. Investig. Dermatol 39 (1962) 387–393. [PubMed: 13933249]

[2]. Aoki Y, Morishita M, Asai K, Akikusa B, Hosoda S, Takayama K, Regiondependent role of the mucous/glycocalyx layers in insulin permeation across rat small intestinal membrane, Pharm. Res 22 (2005) 1854–1862. [PubMed: 16041494]

[3]. Prausnitz MR, Engineering microneedle patches for vaccination and drug delivery to skin, Annu. Rev. Chem. Biomol 8 (2017) 177–200.

[4]. Ye Y, Yu J, Wen D, Kahkoska AR, Gu Z, Polymeric microneedles for transdermal protein delivery, Adv. Drug Deliv. Rev 127 (2018) 106–118. [PubMed: 29408182]

[5]. Henry S, McAllister DV, Allen MG, Prausnitz MR, Microfabricated microneedles: a novel approach to transdermal drug delivery, J. Pharm. Sci 87 (1998) 922–925. [PubMed: 9687334]

[6]. Bal SM, Caussin J, Pavel S, Bouwstra JA, In vivo assessment of safety of microneedle arrays in human skin, Eur. J. Pharm. Sci 35 (2008) 193–202.

[7]. Chen M-C, Wang K-W, Chen D-H, Ling M-H, Liu C-Y, Remotely triggered release of small molecules from LaB6@SiO2-loaded polycaprolactone microneedles, Acta Biomater. 13 (2015) 344–353. [PubMed: 25463507]

[8]. Kim Y-C, Quan F-S, Yoo D-G, Compans RW, Kang S-M, Prausnitz MR, Improved influenza vaccination in the skin using vaccine coated microneedles, Vaccine 27 (2009) 6932–6938. [PubMed: 19761836]

[9]. Yu J, Zhang Y, Ye Y, DiSanto R, Sun W, Ranson D, Ligler FS, Buse JB, Gu Z, Microneedle-array patches loaded with hypoxia-sensitive vesicles provide fast glucose-responsive insulin delivery, Proc. Natl. Acad. Sci. U. S. A 112 (2015) 8260–8265. [PubMed: 26100900]

[10]. Zhu Q, Zarnitsyn VG, Ye L, Wen Z, Gao Y, Pan L, Skountzou I, Gill HS, Prausnitz MR, Yang C, Compans RW, Immunization by vaccine-coated microneedle arrays protects against lethal influenza virus challenge, Proc. Natl. Acad. Sci. U. S. A 106 (2009) 7968–7973. [PubMed: 19416832]

[11]. A.A. Ali CM McCrudden J McCaffrey JW McBride G Cole NJ Dunne T Robson A Kissenpfennig RF Donnelly HO McCarthy, DNA vaccination for cervical cancer; a novel technology platform of RALA mediated gene delivery via polymeric microneedles, Nanomedicine 13 (2017) 921–932. [PubMed: 27979747]

[12]. Lee K, Kim JD, Lee CY, Her S, Jung H, A high-capacity, hybrid electromicroneedle for in-situ cutaneous gene transfer, Biomaterials 32 (2011) 7705–7710. [PubMed: 21764124]

[13]. Wang C, Ye Y, Hochu GM, Sadeghifar H, Gu Z, Enhanced cancer immunotherapy by microneedle patch-assisted delivery of anti-PD1 antibody, Nano Lett. 16 (2016) 2334–2340. [PubMed: 26999507]

[14]. Lee JW, Prausnitz MR, Drug delivery using microneedle patches: not just for skin, Expert Opin. Drug Deliv 15 (2018) 541–543. [PubMed: 29708770]

[15]. Prausnitz MR, Microneedles for transdermal drug delivery, Adv. Drug Deliv. Rev 56 (2004) 581–587. [PubMed: 15019747]

[16]. Prausnitz MR, Langer R, Transdermal drug delivery, Nat. Biotechnol 26 (2008) 1261–1268. [PubMed: 18997767]

[17]. Kim YC, Park JH, Prausnitz MR, Microneedles for drug and vaccine delivery, Adv. Drug Deliv. Rev 64 (2012) 1547–1568. [PubMed: 22575858]

[18]. Yu J, Zhang Y, Kahkoska AR, Gu Z, Bioresponsive transcutaneous patches, Curr. Opin. Biotechnol 48 (2017) 28–32. [PubMed: 28292673]

[19]. Doddaballapur S, Microneedling with dermaroller, J. Cutan. Aesthet. Surg 2 (2009) 110–111. [PubMed: 20808602]

[20]. Gill HS, Prausnitz MR, Coated microneedles for transdermal delivery, J. Control. Release 117 (2007) 227–237. [PubMed: 17169459]

[21]. Gill HS, Prausnitz MR, Coating formulations for microneedles, Pharm. Res 24 (2007) 1369–1380. [PubMed: 17385011]

[22]. Jiang J, Gill HS, Ghate D, McCarey BE, Patel SR, Edelhauser HF, Prausnitz MR, Coated microneedles for drug delivery to the eye, Invest. Ophthalmol. Vis. Sci 48 (2007) 4038–4043. [PubMed: 17724185]

[23]. Laurent PE, Bonnet S, Alchas P, Regolini P, Mikszta JA, Pettis R, Harvey NG, Evaluation of the clinical performance of a new intradermal vaccine administration technique and associated delivery system, Vaccine 25 (2007) 8833–8842. [PubMed: 18023942]

[24]. Ziemssen T, Sylvester L, Rametta M, Ross AP, Patient satisfaction with the new interferon beta-1b autoinjector (BETACONNECT™), Neurol. Ther 4 (2015) 125–136. [PubMed: 26662362]

[25]. Vescovo P, Rettby N, Ramaniraka N, Liberman J, Hart K, Cachemaille A, Piveteau L-D, Zanoni R, Bart P-A, Pantaleo G, Safety, tolerability and efficacy of intradermal rabies immunization with DebioJectTM, Vaccine 35 (2017) 1782–1788. [PubMed: 28317660]

[26]. McAllister DV, Allen MG, Prausnitz MR, Microfabricated microneedles for gene and drug delivery, Annu. Rev. Biomed. Eng 2 (2000) 289–313. [PubMed: 11701514]

[27]. Wilke N, Hibert C, O'Brien J, Morrissey A, Silicon microneedle electrode array with temperature monitoring for electroporation, Sensor. Actuat. a-Phys 123 (2005) 319–325.

[28]. Chabri F, Bouris K, Jones T, Barrow D, Hann A, Allender C, Brain K, Birchall J, Microfabricated silicon microneedles for nonviral cutaneous gene delivery, Br. J. Dermatol 150 (2004) 869–877. [PubMed: 15149498]

[29]. Ji J, Tay FE, Miao J, Microfabricated hollow microneedle array using ICP etcher, J. Phys. Conf. Ser 34 (2006) 1132IOP Publishing.

[30]. Zhang Y.-h., Campbell SA, Preparation of hollow hafnium oxide microneedles for transdermal drug delivery, International Congress on Image and Signal Processing, BioMedical Engineering and Informatics (CISP-BMEI), IEEE 2016, pp. 1756–1760.

[31]. Mukerjee E, Collins SD, Isseroff RR, Smith RL, Microneedle array for transdermal biological fluid extraction and in situ analysis, Sensor. Actuat. a-Phys 114 (2004) 267–275.

[32]. Roxhed N, Griss P, Stemme G, A method for tapered deep reactive ion etching using a modified Bosch process, J. Micromech. Microeng 17 (2007) 1087–1092.

[33]. Griss P, Stemme G, Side-opened out-of-plane microneedles for microfluidic transdermal liquid transfer, J. Microelectromech. S 12 (2003) 296–301.

[34]. Bassous E, Fabrication of novel three-dimensional microstructures by the anisotropic etching of (100) and (110) silicon, IEEE T. Electron Dev 25 (1978) 1178–1185.

[35]. Bassous E, Baran EF, The fabrication of high precision nozzles by the anisotropic etching of (100) silicon, J. Electrochem. Soc 125 (1978) 1321–1327.

[36]. <cos/>Trimmer W, Ling P, Chin C-K, Orton P, Gaugler R, Hashmi S, Hashmi G, Brunett B, Reed M, Injection of DNA into plant and animal tissues with micromechanical piercing structures, Micro Electro Mechanical Systems, 1995, MEMS'95, Proceedings. IEEE, IEEE 1995, p. 111.

[37]. Wilke N, Reed ML, Morrissey A, The evolution from convex corner undercut towards microneedle formation: theory and experimental verification, J. Micromech. Microeng 16 (2006) 808–814.

[38]. Lee J, Kim DH, Lee KJ, Seo IH, Park SH, Jang EH, Park Y, Youn YN, Ryu W, Transfer-molded wrappable microneedle meshes for perivascular drug delivery, J. Control. Release 268 (2017) 237–246. [PubMed: 29030224]

[39]. Wilke N, Morrissey A, Silicon microneedle formation using modified mask designs based on convex corner undercut, J. Micromech. Microeng 17 (2006) 238.

[40]. Shikida M, Odagaki M, Todoroki N, Ando M, Ishihara Y, Ando T, Sato K, Nonphotolithographic pattern transfer for fabricating arrayed three-dimensional microstructures by chemical anisotropic etching, Sensor. Actuat. a-Phys 116 (2004) 264–271.

[41]. Harvey EC, Rumsby PT, Fabrication Techniques and their Application to Produce Novel Micromachined Structures and Devices using Excimer Laser Projection, Micromachining and Microfabrication Process Technology III, International Society for Optics and Photonics, 1997 26–33.

[42]. Omatsu T, Chujo K, Miyamoto K, Okida M, Nakamura K, Aoki N, Morita R, Metal microneedle fabrication using twisted light with spin, Opt. Express 18 (2010) 17967–17973. [PubMed: 20721183]

[43]. Kim K, Park DS, Lu HM, Che W, Kim K, Lee JB, Ahn CH, A tapered hollow metallic microneedle array using backside exposure of SU-8, J. Micromech. Microeng 14 (2004) 597–603.

[44]. Park JH, Yoon YK, Choi SO, Prausnitz MR, Allen MG, Tapered conical polymer microneedles fabricated using an integrated lens technique for transdermal drug delivery, IEEE T. Bio-Med. Eng 54 (2007) 903–913.

[45]. Luzuriaga MA, Berry DR, Reagan JC, Smaldone RA, Gassensmith JJ, Biodegradable 3D printed polymer microneedles for transdermal drug delivery, Lab. Chip 18 (2018) 1223–1230. [PubMed: 29536070]

[46]. Pere CPP, Economidou SN, Lall G, Ziraud C, Boateng JS, Alexander BD, Lamprou DA, Douroumis D, 3D printed microneedles for insulin skin delivery, Int. J. Pharm 544 (2018) 425–432. [PubMed: 29555437]

[47]. Ochoa M, Zhou J, Rahimi R, Badwaik V, Thompson D, Ziaie B, Rapid 3D-Print-and-Shrink Fabrication of Biodegradable Microneedles with Complex Geometries, 2015 Transducers-2015 18th International Conference on Solid-State Sensors, Actuators and Microsystems (TRANSDUCERS), IEEE, 2015 1251–1254.

[48]. Lee K, Lee HC, Lee DS, Jung H, Drawing lithography: three-dimensional fabrication of an ultrahigh-aspect-ratio microneedle, Adv. Mater 22 (2010) 483–486. [PubMed: 20217738]

[49]. Choi CK, Lee KJ, Youn YN, Jang EH, Kim W, Min BK, Ryu W, Spatially discrete thermal drawing of biodegradable microneedles for vascular drug delivery, Eur. J. Pharm. Biopharm 83 (2013) 224–233. [PubMed: 23201049]

[50]. Lee K, Park SH, Lee J, Ryu S, Joo C, Ryu W, Three-step thermal drawing for rapid prototyping of highly customizable microneedles for vascular tissue insertion, Pharmaceutics 11 (2019) 100.

[51]. Lee KJ, Park SH, Lee JY, Joo HC, Jang EH, Youn Y-N, Ryu W, Perivascular biodegradable microneedle cuff for reduction of neointima formation after vascular injury, J. Control. Release 192 (2014) 174–181. [PubMed: 25025286]

[52]. Lin YH, Lee IC, Hsu WC, Hsu CH, Chang KP, Gao SS, Rapid fabrication method of a microneedle mold with controllable needle height and width, Biomed. Microdevices 18 (2016), 85.

[53]. Kim JD, Kim M, Yang H, Lee K, Jung H, Droplet-born air blowing: novel dissolving microneedle fabrication, J. Control. Release 170 (2013) 430–436. [PubMed: 23742882]

[54]. Vecchione R, Coppola S, Esposito E, Casale C, Vespini V, Grilli S, Ferraro P, Netti PA, Electro-drawn drug-loaded biodegradable polymer microneedles as a viable route to hypodermic injection, Adv. Funct. Mater 24 (2014) 3515–3523.

[55]. Chen ZP, Ren L, Li JY, Yao LB, Chen Y, Liu B, Jiang LL, Rapid fabrication of microneedles using magnetorheological drawing lithography, Acta Biomater. 65 (2018) 283–291. [PubMed: 29107057]

[56]. Yang H, Kim S, Kang G, Lahiji SF, Jang M, Kim YM, Kim JM, Cho SN, Jung H, Centrifugal lithography: self-shaping of polymer microstructures encapsulating biopharmaceutics by centrifuging polymer drops, Adv. Health. Mater 6 (2017) 1700326.

[57]. Lee JW, Park JH, Prausnitz MR, Dissolving microneedles for transdermal drug delivery, Biomaterials 29 (2008) 2113–2124. [PubMed: 18261792]

[58]. Raphael AP, Prow TW, Crichton ML, Chen X, Fernando GJ, Kendall MAJS, Targeted, needle-free vaccinations in skin using multilayered, densely-packed dissolving microprojection arrays, Small 6 (2010) 1785–1793. [PubMed: 20665628]

[59]. Sullivan SP, Murthy N, Prausnitz MR, Minimally invasive protein delivery with rapidly dissolving polymer microneedles, Adv. Mater. 20 (2008) 933–938. [PubMed: 23239904]

[60]. Chu LY, R Prausnitz M, Separable arrowhead microneedles, J. Control. Release 149 (2011) 242–249. [PubMed: 21047538]

[61]. Chu LY, Choi SO, R Prausnitz M, Fabrication of dissolving polymer microneedles for controlled drug encapsulation and delivery: bubble and pedestal microneedle designs, J. Pharm. Sci 99 (2010) 4228–238. [PubMed: 20737630]

[62]. Wendorf JR, Ghartey-Tagoe EB, Williams SC, Enioutina E, Singh P, Cleary GW, Transdermal delivery of macromolecules using solid-state biodegradable microstructures, Pharm. Res 28 (2011) 22–30. [PubMed: 20535531]

[63]. Martin CJ, Allender CJ, Brain KR, Morrissey A, Birchall JC, Low temperature fabrication of biodegradable sugar glass microneedles for transdermal drug delivery applications, J. Control. Release 158 (2012) 93–101. [PubMed: 22063007]

[64]. Loizidou EZ, Williams NA, Barrow DA, Eaton MJ, McCrory J, Evans SL, Allender CJ, Structural characterisation and transdermal delivery studies on sugar microneedles: experimental and finite element modelling analyses, Eur. J. Pharm. Biopharm 89 (2015) 224–231. [PubMed: 25481031]

[65]. Kolli CS, Banga AK, Characterization of solid maltose microneedles and their use for transdermal delivery, Pharm. Res 25 (2008) 104–113. [PubMed: 17597381]

[66]. Donnelly RF, Singh TRR, Garland MJ, Migalska K, Majithiya R, McCrudden CM, Kole PL, Mahmood TMT, McCarthy HO, Woolfson AD, Hydrogel-forming microneedle arrays for enhanced transdermal drug delivery, Adv. Funct. Mater 22 (2012) 4879–4890. [PubMed: 23606824]

[67]. Kim M, Jung B, Park J-H, Hydrogel swelling as a trigger to release biodegradable polymer microneedles in skin, Biomaterials 33 (2012) 668–678. [PubMed: 22000788]

[68]. Park JH, Allen MG, Prausnitz MR, Biodegradable polymer microneedles: fabrication, mechanics and transdermal drug delivery, J. Control. Release 104 (2005) 51–66. [PubMed: 15866334]

[69]. Park JH, Allen MG, Prausnitz MR, Polymer microneedles for controlled-release drug delivery, Pharm. Res 23 (2006) 1008–1019. [PubMed: 16715391]

[70]. Tsioris K, Raja WK, Pritchard EM, Panilaitis B, Kaplan DL, Omenetto FG, Fabrication of silk microneedles for controlled-release drug delivery, Adv. Funct. Mater 22 (2012) 330–335.

[71]. Lee J, Park SH, Seo IH, Lee KJ, Ryu W, Rapid and repeatable fabrication of high A/R silk fibroin microneedles using thermally-drawn micromolds, Eur. J. Pharm. Biopharm 94 (2015) 11–19. [PubMed: 25936857]

[72]. Yang SY, O'Cearbhaill ED, Sisk GC, Park KM, Cho WK, Villiger M, Bouma BE, Pomahac B, Karp JM, A bio-inspired swellable microneedle adhesive for mechanical interlocking with tissue, Nat. Commun 4 (2013), 1702. [PubMed: 23591869]

[73]. Chang H, Zheng M, Yu X, Than A, Seeni RZ, Kang R, Tian J, Khanh DP, Liu L, Chen P, Xu C, A swellable microneedle patch to rapidly extract skin interstitial fluid for timely metabolic analysis, Adv. Mater. 29 (2017), 1702243.

[74]. Imaeda K, Bessho K, Shikida M, Sharp Tip-Separable Microneedle Device for Trans-Dermal Drug Delivery Systems, 2015 Transducers - 2015 18th International Conference on Solid-State Sensors, Actuators and Microsystems (TRANSDUCERS) , IEEE, 2015 1715–1718.

[75]. Chen M-C, Huang S-F, Lai K-Y, Ling M-H, Fully embeddable chitosan microneedles as a sustained release depot for intradermal vaccination, Biomaterials 34(2013) 3077–3086. [PubMed: 23369214]

[76]. Dai W, Lian K, Wang W, A quantitative study on the adhesion property of cured SU-8 on various metallic surfaces, Microsyst. Technol 11 (2005) 526–534.

[77]. Song HB, Lee KJ, Seo IH, Lee JY, Lee S-M, Kim JH, Kim JH, Ryu W, Impact insertion of transfer-molded microneedle for localized and minimally invasive ocular drug delivery, J. Control. Release 209 (2015) 272–279. [PubMed: 25937320]

[78]. Hyun Park S, Hyun Jo D, Sik Cho C, Lee K, Hyoung Kim J, Ryu S, Joo C, Hun Kim J, Ryu W, Depthwise-controlled scleral insertion of microneedles for drug delivery to the back of the eye, Eur. J. Pharm. Biopharm 133 (2018) 31–41. [PubMed: 30267835]

[79]. Lee K, Beom Song H, Cho W, Hyoung Kim J, Hun Kim J, Ryu W, Intracorneal injection of a detachable hybrid microneedle for sustained drug delivery, Acta Biomater. 80 (2018) 48–57. [PubMed: 30267886]

[80]. Vasylieva N, Marinesco S, Barbier D, Sabac A, Silicon/SU8 multi-electrode microneedle for in vivo neurochemical monitoring, Biosens. Bioelectron 72 (2015) 148–155. [PubMed: 25978443]

[81]. Lee HJ, Son Y, Kim D, Kim YK, Choi N, Yoon E-S, Cho I-J, A new thin silicon microneedle with an embedded microchannel for deep brain drug infusion, Sensor. Actuat. B-Chem 209 (2015) 413–422.

[82]. Narbutovskih M, Wilson CJ, Ormeggi A, Fracture testing of silicon microcantilever beams, J. Appl. Phys. B-Chem 79 (1996) 2386–2398.

[83]. O'Mahony C, Structural characterization and in-vivo reliability evaluation of silicon microneedles, Biomed. Microdevices 16 (2014) 333–343. [PubMed: 24487507]

[84]. Bayliss SC, Harris PJ, Buckberry LD, Rousseau C, Phosphate and cell growth on nanostructured semiconductors, J. Mater. Sci. Lett 16 (1997) 737–740.

[85]. Millard DR Jr., Maisels DO, Silicon granuloma of the skin and subcutaneous tissues, Am. J. Surg 112 (1966) 119–123. [PubMed: 5936639]

[86]. Winslow BD, Christensen MB, Yang W-K, Solzbacher F, Tresco PA, A comparison of the tissue response to chronically implanted Parylene-C-coated and uncoated planar silicon microelectrode arrays in rat cortex, Biomaterials 31 (2010) 9163–9172. [PubMed: 20561678]

[87]. Nishinaka Y, Jun R, Prihandana GS, Miki N, Fabrication of polymer microneedle electrodes coated with Nanoporous Parylene, Jpn. J. Appl. Phys. 52 (2013).

[88]. Chen Q, Thouas GA, Metallic implant biomaterials, Mat. Sci. Eng. R 87 (2015) 1–57.

[89]. Cormier M, Johnson B, Ameri M, Nyam K, Libiran L, Zhang DD, Daddona P, Transdermal delivery of desmopressin using a coated microneedle array patch system, J. Control. Release 97 (2004) 503–511. [PubMed: 15212882]

[90]. Parker E, Rao M, Turner K, Meinhart C, MacDonald N, Bulk Micromachined Titanium Microneedles, J. Microelectromech. Syst 16 (2007) 289–295.

[91]. Mineta T, Tanahashi Y, Makino E, Toh S, Kawashima T, Shibata T, Thermal-type blood flow sensor on titanium microneedle, Sensor. Mater 20 (2008) 341–349.

[92]. Gaines AR, Pierce LR, Bernhardt PA, Fatal Iatrogenic Hypoglycemia: Falsely Elevated Blood Glucose Readings with a Point-of-Care Meter Due to a Maltose-Containing Intravenous Immune Globulin Product, FDA, Safety Availability Bulletin, 2009.

[93]. Ameers MJ, Excipient-drug interactions in parenteral formulations, J. Pharm. Sci 91 (2002) 2283–2300. [PubMed: 12379914]

[94]. Schneider AS, Schettler A, Markowski A, Luettig B, Momma M, Seipt C, Hadem J, Wilhelmi MJCN, Assessment of xylitol serum levels during the course of parenteral nutrition including xylitol in intensive care patients: a case control study, Clin. Nutr 33 (2014) 483–488. [PubMed: 23916161]

[95]. Dhar N, Akhlaghi SP, Tam KC, Biodegradable and biocompatible polyampholyte microgels derived from chitosan, carboxymethyl cellulose and modified methyl cellulose, Carbohydr. Polym 87 (2012) 101–109.

[96]. Croisier F, Jérôme C, Chitosan-based biomaterials for tissue engineering, Eur. Polym. J 49 (2013) 780–792.

[97]. Necas J, Bartosikova L, Brauner P, Kolar J, Hyaluronic acid (hyaluronan): a review, Vet. Med-Czech 53 (2008) 397–411.

[98]. Alrifaiy A, OA Lindahl K Ramser, Polymer-based microfluidic devices for pharmacy, biology and tissue engineering, Polymers 4 (2012) 1349–1398.

[99]. Frazer RQ, Byron RT, Osborne PB, West KP, PMMA: an essential material in medicine and dentistry, J. Long-Term Eff. Med. Implants 15 (2005).

[100]. Jin CY, Han MH, Lee SS, Choi YH, Mass producible and biocompatible microneedle patch and functional verification of its usefulness for transdermal drug delivery, Biomed. Microdevices 11 (2009) 1195. [PubMed: 19609679]

[101]. Oh J-H, Park H-H, Do K-Y, Han M, Hyun D-H, Kim C-G, Kim C-H, Lee SS, Hwang S-J, Shin S-C, Influence of the delivery systems using a microneedle array on the permeation of a hydrophilic molecule, calcein, Eur. J. Pharm. Biopharm 69 (2008) 1040–1045. [PubMed: 18411045]

[102]. Tijero M, Gabriel G, Caro J, Altuna A, Hernandez R, Villa R, Berganzo J, Blanco F, Salido R, Fernandez L, SU-8 microprobe with microelectrodes for monitoring electrical impedance in living tissues, Biosens. Bioelectron. 24 (2009) 2410–2416. [PubMed: 19167206]

[103]. Cho S-H, Lu HM, Cauller L, Romero-Ortega MI, Lee J-B, Hughes GA, Biocompatible SU-8-based microprobes for recording neural spike signals from regenerated peripheral nerve fibers, IEEE Sensors J. 8 (2008) 1830–1836.

[104]. Xue N, Chang SP, Lee J-B, A SU-8-based compact implantable wireless pressure sensor for intraocular pressure sensing application, 2011 Annual International Conference of the IEEE Engineering in Medicine and Biology Society, IEEE 2011, pp. 2854–2857.

[105]. Nemani KV, Moodie KL, Brennick JB, Su A, Gimi B, In vitro and in vivo evaluation of SU-8 biocompatibility, Mater. Sci. Eng. C 33 (2013) 4453–4459.

[106]. Baker MI, Walsh SP, Schwartz Z, Boyan BD, A review of polyvinyl alcohol and its uses in cartilage and orthopedic applications, J. Biomed. Mater. Res. B Appl. Biomater 100 (2012) 1451–1457. [PubMed: 22514196]

[107]. Montezuma SR, Loewenstein J, Scholz C, Rizzo JF, Biocompatibility of materials implanted into the subretinal space of Yucatan pigs, Invest. Ophthalmol. Vis. Sci 47 (2006) 3514–3522. [PubMed: 16877423]

[108]. El-Mohdy HA, Ghanem S, Biodegradability, antimicrobial activity and properties of PVA/PVP hydrogels prepared by γ-irradiation, J. Polym. Res 16 (1) (2009).

[109]. Grayson AC, Voskerician G, Lynn A, Anderson JM, Cima MJ, Langer R, Differential degradation rates in vivo and in vitro of biocompatible poly (lactic acid) and poly (glycolic acid) homo-and co-polymers for a polymeric drug-delivery microchip, J. Biomater. Sci. Polym. Ed 15 (2004) 1281–1304. [PubMed: 15559850]

[110]. Choi CK, Kim JB, Jang EH, Youn Y-N, Ryu WH, Curved biodegradable microneedles for vascular drug delivery, Small 8 (2012) 2483–2488. [PubMed: 22628194]

[111]. Urtti A, Challenges and obstacles of ocular pharmacokinetics and drug delivery, Adv. Drug Deliv. Rev 58 (2006) 1131–1135. [PubMed: 17097758]

[112]. Vaishya RD, Khurana V, Patel S, Mitra AK, Controlled ocular drug delivery with nanomicelles, Wiley Interdiscip. Rev. Nanomed. Nanobiotechnol 6 (2014) 422–437. [PubMed: 24888969]

[113]. Kim YC, Grossniklaus HE, Edelhauser HF, Prausnitz MR, Intrastromal delivery of bevacizumab using microneedles to treat corneal neovascularization, Invest. Ophthalmol. Vis. Sci 55 (2014) 7376–7386. [PubMed: 25212779]

[114]. Khandan O, Kahook MY, Rao MP, Fenestrated microneedles for ocular drug delivery, Sensor. Actuat. B-Chem 223 (2016) 15–23.

[115]. Thakur RRS, Tekko IA, Al-Shammari F, Ali AA, McCarthy H, Donnelly RF, Rapidly dissolving polymeric microneedles for minimally invasive intraocular drug delivery, Drug Deliv. Transl. Res 6 (2016) 800–815. [PubMed: 27709355]

[116]. Bhatnagar S, Saju A, Cheerla KD, Gade SK, Garg P, Venuganti VVK, Corneal delivery of besifloxacin using rapidly dissolving polymeric microneedles, Drug Deliv. Transl. Res 8 (2018) 473–483. [PubMed: 29288357]

[117]. Than A, Liu C, Chang H, Phan Khanh D, Cheung CMG, Xu C, Wang X, Chen P, Self-implantable double-layered micro-drug-reservoirs for efficient and controlled ocular drug delivery, Nat. Commun 9 (2018).

[118]. Jonas JB, Spandau UH, Schlichtenbrede F, Short-term complications of intravitreal injections of triamcinolone and bevacizumab, Eye 22 (2008) 590–591. [PubMed: 18292795]

[119]. Patel SR, Lin ASP, Edelhauser HF, Prausnitz MR, Suprachoroidal drug delivery to the back of the eye using hollow microneedles, Pharm. Res 28 (2011) 166–176. [PubMed: 20857178]

[120]. Kim YC, Oh KH, Edelhauser HF, Prausnitz MR, Formulation to target delivery to the ciliary body and choroid via the suprachoroidal space of the eye using microneedles, Eur. J. Pharm. Biopharm 95 (2015) 398–406. [PubMed: 26036448]

[121]. Chiang B, Venugopal N, Edelhauser HF, Prausnitz MR, Distribution of particles, small molecules and polymeric formulation excipients in the suprachoroidal space after microneedle injection, Exp. Eye Res 153 (2016) 101–109. [PubMed: 27742547]

[122]. Lee CY, Lee K, You YS, Lee SH, Jung H, Tower microneedle via reverse drawing lithography for innocuous intravitreal drug delivery, Adv. Health. Mater 2 (2013) 812–816.

[123]. Newby AC, Zaltsman AB, Molecular mechanisms in intimal hyperplasia, J. Pathol 190 (2000) 300–309. [PubMed: 10685064]

[124]. Kavros SJ, Delis KT, Turner NS, Voll AE, Liedl DA, Gloviczki P, Rooke TW, Improving limb salvage in critical ischemia with intermittent pneumatic compression: a controlled study with 18-month follow-up, J. Vasc. Surg 47 (2008) 543–549. [PubMed: 18295105]

[125]. Kelly B, Melhem M, Zhang J, Kasting G, Li J, Krishnamoorthy M, Heffelfinger S, Rudich S, Desai P, Roy-Chaudhury P, Perivascular paclitaxel wraps block arteriovenous graft stenosis in a pig model, Nephrol. Dial. Transpl 21 (2006) 2425–2431.

[126]. Signore PE, Machan LS, Jackson JK, Burt H, Bromley P, Wilson JE, McManus BM, Complete inhibition of intimal hyperplasia by perivascular delivery of paclitaxel in balloon-injured rat carotid arteries, J. Vasc. Interv. Radiol 12 (2001) 79–88. [PubMed: 11200358]

[127]. Kohler TR, Toleikis PM, Gravett DM, Avelar RL, Inhibition of neointimal hyperplasia in a sheep model of dialysis access failure with the bioabsorbable Vascular Wrap paclitaxel-eluting mesh, J. Vasc. Surg 45 (2007) 1029–1038. [PubMed: 17466798]

[128]. Paulson WD, Kipshidze N, Kipiani K, Beridze N, DeVita MV, Shenoy S, Iyer SS, Safety and efficacy of local periadventitial delivery of sirolimus for improving hemodialysis graft patency: first human experience with a sirolimus-eluting collagen membrane (Coll-R), Nephrol. Dial. Transplant 27 (2012) 1219–1224. [PubMed: 22241793]

[129]. Kim D-H, Jang EH, Lee K, Lee JY, Park SH, Seo IH, Lee KW, Lee SH, Ryu WH, Youn Y-N, A biodegradable microneedle cuff for comparison of drug effects through perivascular delivery to balloon-injured arteries, Polymers 9 (2017).

[130]. Owens CD, Gasper WJ, Walker JP, Alley HF, Conte MS, Grenon SM, Safety and feasibility of adjunctive dexamethasone infusion into the adventitia of the femoropopliteal artery following endovascular revascularization, J. Vasc. Surg 59 (2014) 1016–1023. [PubMed: 24423476]

[131]. Peppas A, Seward K, Van Wygerden K, Conditt G, Tellez A, Rousselle S, Kaluza G, Granada J, Prevention of restenosis with adventitial delivery of Torisel via Mercator MedSystems bullfrog catheter in femoral arteries of swine, J. Am. Coll. Cardiol 70 (18 Supplement) (2017) B323.

[132]. Lee K, Lee SG, Jang I, Park SH, Yang D, Seo IH, Bong S-K, An DH, Lee MK, Jung IK, Jang YH, Kim JS, Ryu W, Linear micro-patterned drug eluting balloon (LMDEB) for enhanced endovascular drug delivery, Sci. Rep 8 (2018).

[133]. Traverso G, Schoellhammer CM, Schroeder A, Maa R, Lauwers GY, Polat BE, Anderson DG, Blankschtein D, Langer R, Microneedles for drug delivery via the gastrointestinal tract, J. Pharm. Sci 104 (2015) 362–367. [PubMed: 25250829]

[134]. Ma Y, Boese SE, Luo Z, Nitin N, Gill HS, Drug coated microneedles for minimally-invasive treatment of oral carcinomas: development and in vitro evaluation, Biomed. Microdevices 17 (2015) 44. [PubMed: 25787934]

[135]. Paderni C, Compilato D, Giannola LI, Campisi G, Oral local drug delivery and new perspectives in oral drug formulation, Oral Surg. Oral Med. Oral Pathol. Oral Radiol 114(2012) E25–E34.

[136]. Patel VF, Liu F, Brown MB, Advances in oral transmucosal drug delivery, J. Control. Release 153 (2011) 106–116. [PubMed: 21300115]

[137]. Serpe L, Jain A, de Macedo CG, Volpato MC, Groppo FC, Gill HS, Franz-Montan M, Influence of salivary washout on drug delivery to the oral cavity using coated microneedles: An in vitro evaluation, Eur. J. Pharm. Sci 93 (2016) 215–223. [PubMed: 27523787]

[138]. Yun A, Seward K, Delivery of Agents by Microneedle Catheter, Google Patents, 2008.

[139]. Versi E, Method and Device for Delivering Drug to the Trigone of the Bladder, Google Patents, 2011.

[140]. Wang N, Zhen Y, Jin Y, Wang X, Li N, Jiang S, Wang T, Combining different types of multifunctional liposomes loaded with ammonium bicarbonate to fabricate microneedle arrays as a vaginal mucosal vaccine adjuvant-dual delivery system (VADDS), J. Control. Release 246 (2017) 12–29. [PubMed: 27986552]

[141]. Tang J, Wang J, Huang K, Ye Y, Su T, Qiao L, Hensley MT, Caranasos TG, Zhang J, Gu Z, Cheng K, Cardiac Cell-Integrated Microneedle Patch for Treating Myocardial Infarction, Sci. Adv 4 (2018)eaat9365. [PubMed: 30498778]

[142]. Levin Y, Kochba E, Hung I, Kenney R, Intradermal vaccination using the novel microneedle device MicronJet600: past, present, and future, Hum. Vaccin. Immunother 11 (2015) 991–997. [PubMed: 25745830]

[143]. Yuzhakov VV, Method of making microneedle array and device for applying microneedle array to skin, Google Patents (2013).

[144]. Fuller S, Lebowitz M, Stewart S, Walker S, Ghanbari H, Bohlke A, Burton S, Chu L, Hua V, Enhanced immunogenicity of a nanoparticle therapeutic cancer vaccine targeting HAAH delivered intradermally using 3M's hollow microstructured transdermal system (hMTS), J. Immunother. Cancer 3 (2015), P433.

[145]. Dick LA, Paul S, Innovative drug delivery technology to meet evolving need of biologics & small moledules, 56, ONdrugDelivery Magazine, 2019 4–6.

[146]. Kim YC, Edelhauser HF, Prausnitz MR, Targeted delivery of antiglaucoma drugs to the supraciliary space using microneedles, Invest. Ophthalmol. Vis. Sci 55 (2014) 7387–7397. [PubMed: 25212782]

[147]. Arya J, Prausnitz MR, Microneedle patches for vaccination in developing countries, J. Control. Release 240 (2016) 135–141. [PubMed: 26603347]

[148]. Marshall S, Sahm LJ, Moore AC, The success of microneedle-mediated vaccine delivery into skin, Hum. Vaccin. Immunother 12 (2016) 2975–2983. [PubMed: 27050528]

[149]. Miller PR, Skoog SA, Edwards TL, Wheeler DR, Xiao X, Brozik SM, Polsky R, Narayan RJ, Hollow microneedle-based sensor for multiplexed transdermal electrochemical sensing, JoVE (Journal of Visualized Experiments) 64 (2012) e4067.

[150]. Ciechanowska A, Ladyzynski P, Wojcicki JM, Sabalinska S, Krzymien J, Pulawska E, Karnafel W, Foltynski P, Kawiak J, Microdialysis monitoring of glucose, lactate, glycerol, and pyruvate in patients with diabetic ketoacidosis, Int. J. Artif. Organs 36 (2013) 869–877. [PubMed: 24362895]

[151]. Xue P, Zhang L, Xu Z, Yan J, Gu Z, Kang Y, Blood sampling using microneedles as a minimally invasive platform for biomedical diagnostics, Appl. Mater. Today 13 (2018) 144–157.

[152]. Mandal A, Boopathy AV, Lam LKW, Moynihan KD, Welch ME, Bennett NR, Turvey ME, Thai N, Van JH, Love JC, Hammond PT, Irvine DJ, Cell and fluid sampling microneedle patches for monitoring skin-resident immunity, Sci. Transl. Med 10 (2018).

[153]. Pickup JC, Freeman SC, Sutton AJ, Glycaemic control in type 1 diabetes during real time continuous glucose monitoring compared with self monitoring of blood glucose: meta-analysis of randomised controlled trials using individual patient data, Br. Med. J 343 (2011) d3805. [PubMed: 21737469]

[154]. UK Prospective Diabetes Study (UKPDS) Group, Intensive blood-glucose control with sulphonylureas or insulin compared with conventional treatment and risk of complications in patients with type 2 diabetes (UKPDS 33), Lancet 352 (1998) 837–853. [PubMed: 9742976]

[155]. Coyle S, Curto VF, Benito-Lopez F, Florea L, Diamond D, Wearable bio and chemical sensors, Wearable Sensors, Elsevier 2015, pp. 65–83.

[156]. Jina A, Tierney MJ, Tamada JA, McGill S, Desai S, Chua B, Chang A, Christiansen M, Design, development, and evaluation of a novel microneedle arraybased continuous glucose monitor, J. Diabetes Sci. Technol 8 (2014) 483–487. [PubMed: 24876610]
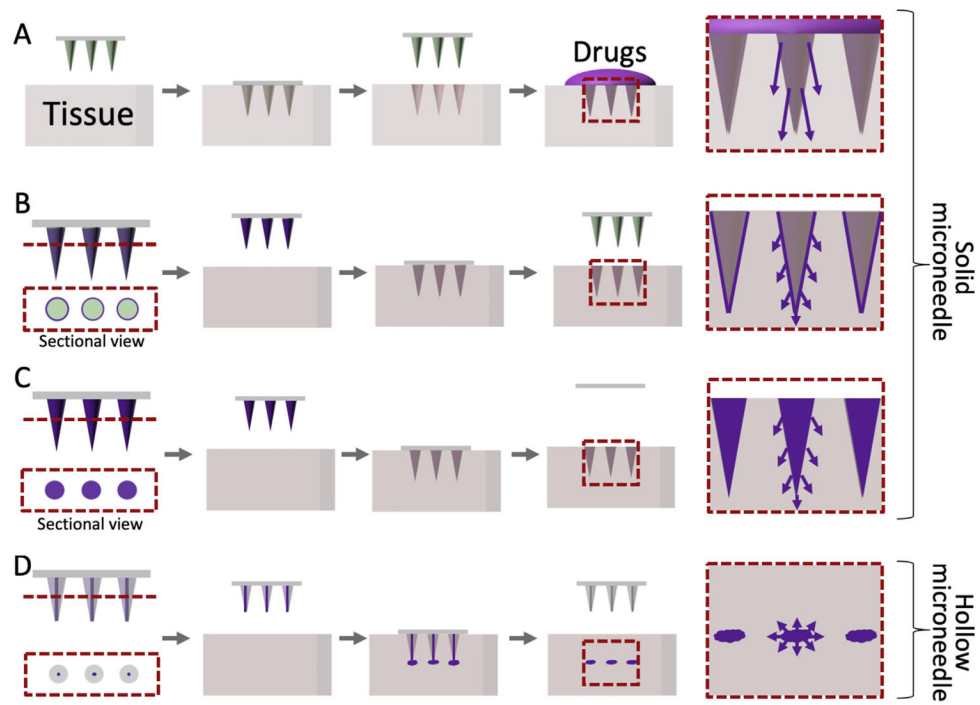
Fig.1.
Illustration of microneedle (MN) types and drug flows. (A) Bare solid MNs providing channels to enhance drug permeability. (B) Drug-coated MNs. (C) Dissolving or biodegradable MNs. (D) Hollow MNs to inject liquid.
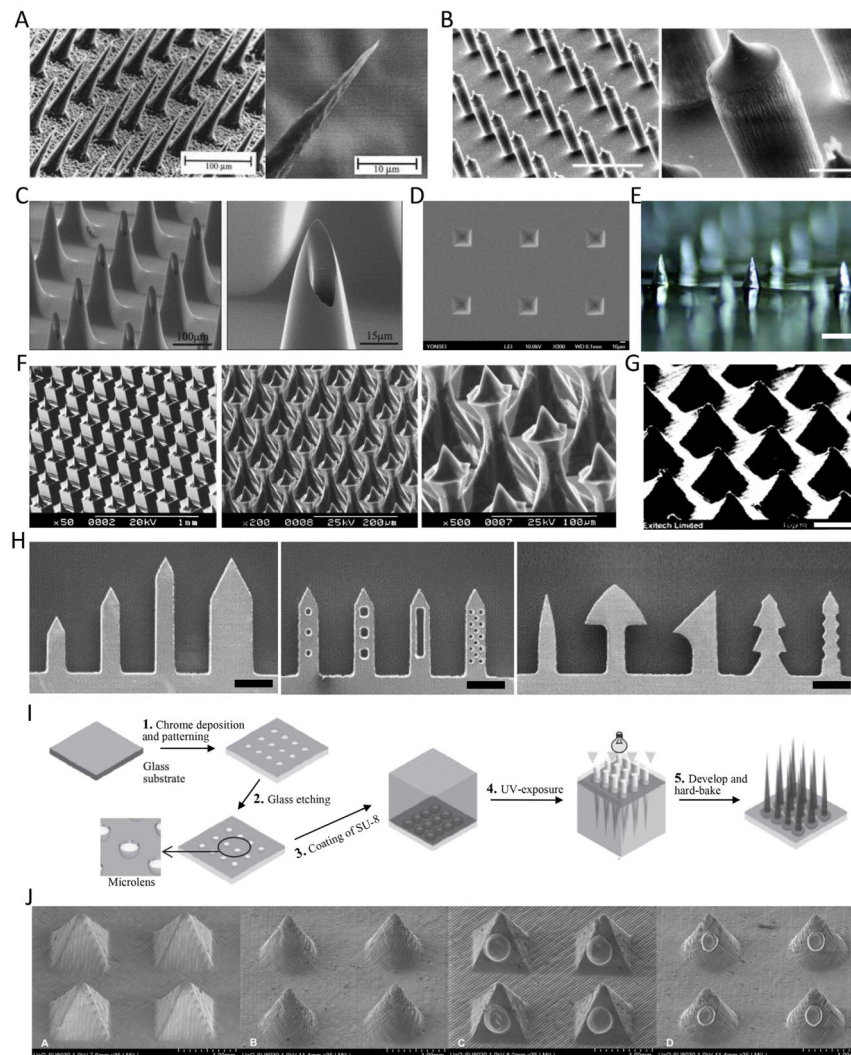
Fig. 2.
Different designs of microfabricated microneedles (MNs). (A) The first MN array fabricated by deep reactive ion etching [5] Copyright (1998) Elsevier. (B) An isotropically etched MN array through the Bosch process [28] (scale bar = 200 μm (left), 20 μm (right)) Copyright (2004) John Wiley and Sons. (C) A hollow and tapered MN array for extraction of biological fluids [31] Copyright (2004) Elsevier. (D) Pyramidal MN cavities tapered at 54.72° after KOH wet etching. (E) A male MN array after KOH wet etching [38] (scale bar = 500 μm) Copyright (2017) Elsevier. (F) Complex structure of MNs through combinatorial dicing – wet etching [40] Copyright (2004) Elsevier. (G) An ablated MN array using excimer laser [41] (scale bar = 40 μm) Copyright (1997) Society of Photo-Optical Instrumentation Engineers (SPIE). (H) Laser cut planar MN [20] Copyright (2007) Elsevier. (I) Schematic of integrated lens process to fabricate tapered-cone MNs [44] Copyright (2005) Elsevier. (J) 3D printed pyramidal- and cone-shaped MNs using stereolithography. Lower two images are insulin coated MNs [46] Copyright (2018) Elsevier. All figures were adopted with permission.
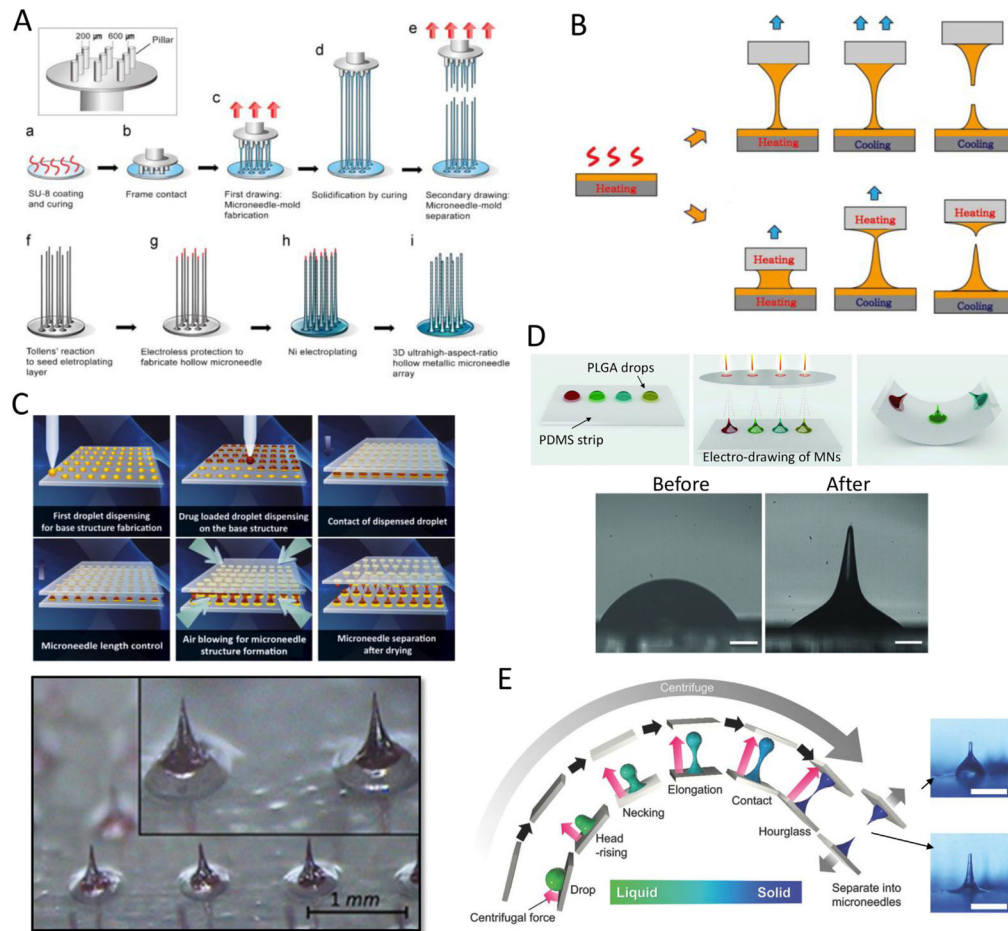
Fig. 3.
Drawing lithography technologies for microneedle (MN) fabrication. (A) Ultra-high aspect ratio MN arrays by SU-8 drawing and Ni electroplating [48] Copyright (2010) John Wiley and Sons. (B) Spatially discrete and thermal drawing for specific body profile of MNs [49] Copyright (2013) Elsevier. (C) Droplet-born air blowing-based drawing lithography for developing MNs containing biological drugs [53] Copyright (2013) Elsevier. (D) Electro-drawing process for drawing PLGA biodegradable MNs [54] (scale bar = 200 μm) Copyright (2014) John Wiley and Sons. (E) Centrifugal lithography to fabricate MN encapsulating biopharmaceutics [56] (scale bar = 500 μm) Copyright (2017) John Wiley and Sons. All figures were adopted with permission.
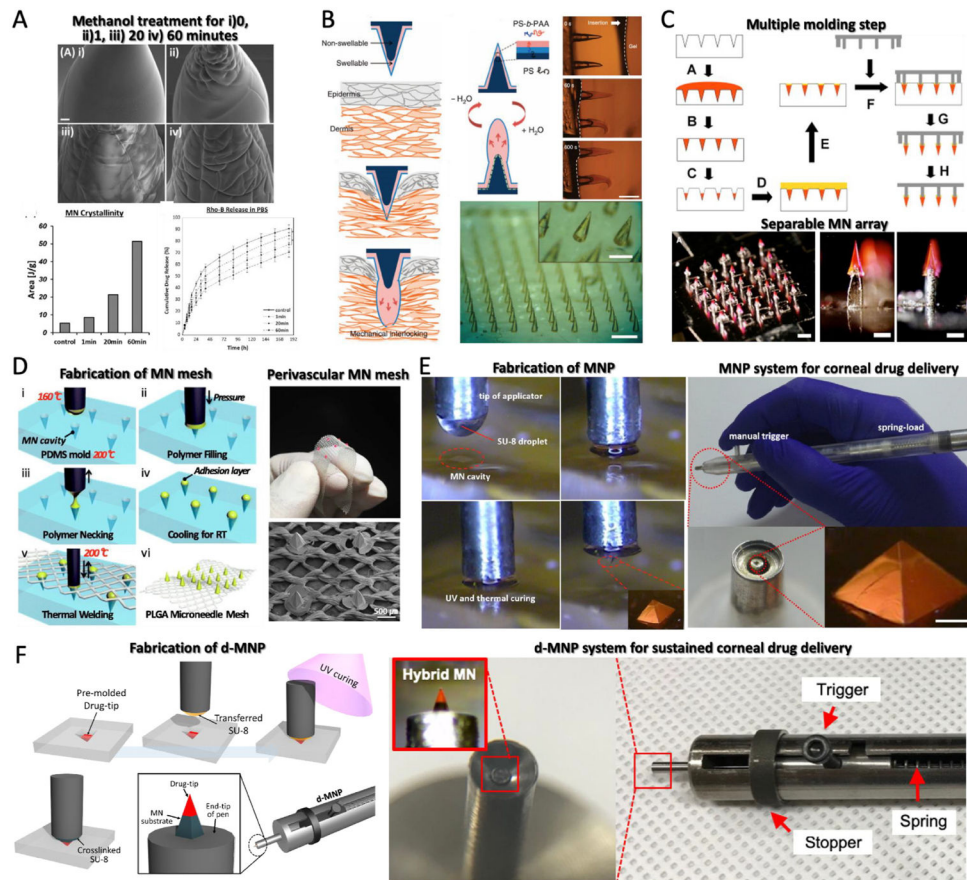
Fig. 4.
(A) Silk fibroin (SF) microneedles (MNs) and controlling drug release profile by varying the degree of crystallinity of SF [71] (scale bar = 10 μm) Copyright (2015) Elsevier. (B) Wound-interlocking MN array consisting of a swellable polystyrene and polyacrylic acid (PS-b-PAA) tip and a non-swellable PS core [72] (scale bar = 500 μm) Copyright (2013) Springer Nature. (C) MNs having separable arrowheads onto the arrays of metal shafts [60] (scale bar = 1 mm (right) 300 μm (mid and left)) Copyright (2011) Elsevier. (D) Polymeric welding process of wrappable MN mesh for perivascular drug delivery [38] Copyright (2017) Elsevier. (E) Coated MN pen (MNP) system for corneal drug delivery [77] (scale bar =100 μm) Copyright (2015) Elsevier. (F) Detachable hybrid MN pen (d-MNP) for sustained corneal drug delivery [79] Copyright (2018) Elsevier. All figures were adopted with permission.
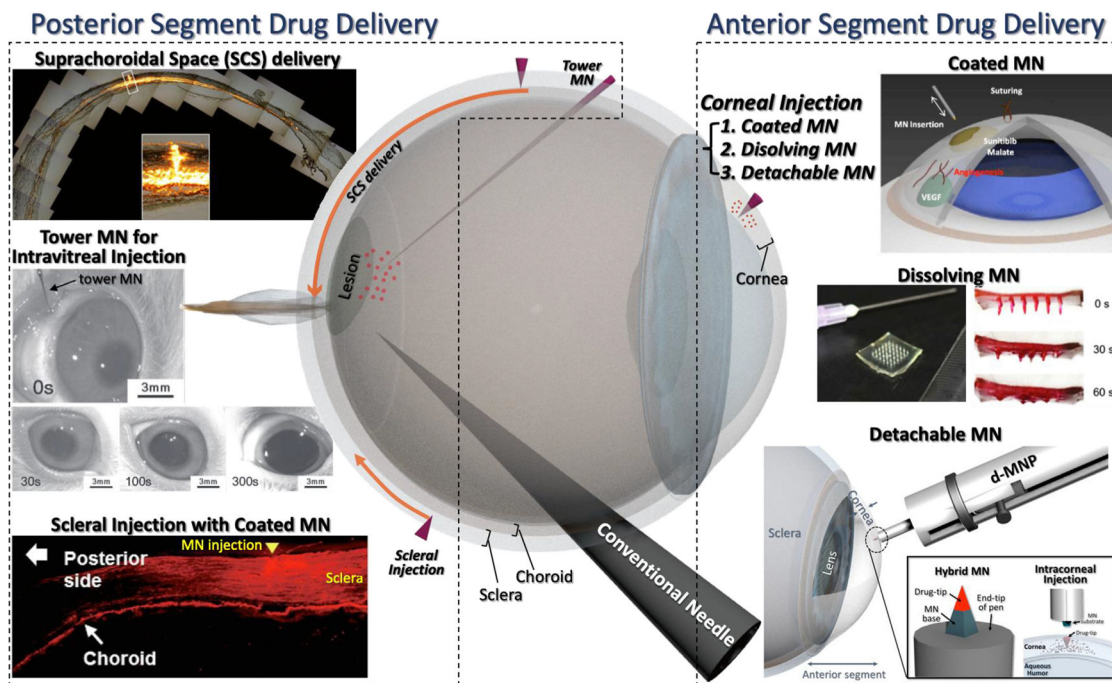
Fig. 5.
Illustration of posterior and anterior segment of the eye and an overview of their ocular drug delivery applications. Three types of corneal drug delivery were conducted in anterior segment drug delivery: 1) Coated microneedle (MN) [77] Copyright (2015) Elsevier, 2) Dissolving MN [116] Copyright (2017) Springer Nature and 3) Detachable MN [79] Copyright (2018) Elsevier. In addition, 3 ways of drug delivery administration to the posterior segment of the eye were conducted: 1) Suprachoroidal space (SCS) delivery [119] Copyright (2010) Springer Nature, 2) Tower MN for intravitreal injection [122] Copyright (2012) John Wiley and Sons and 3) Scleral injection with coated MN [78] Copyright (2018) Elsevier. All figures were adopted with permission.
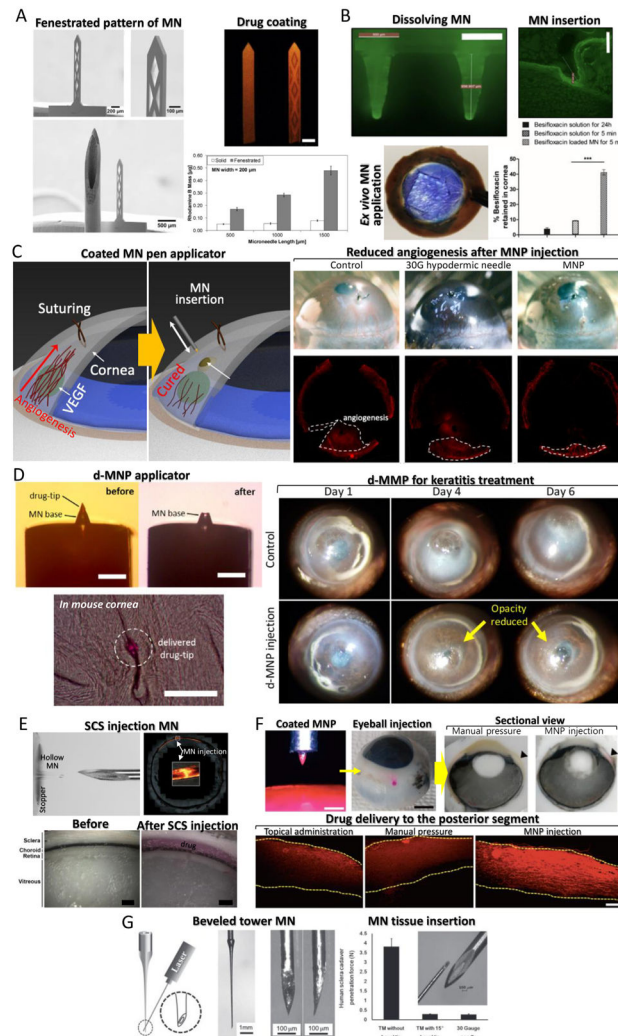
Fig. 6.
Ocular drug delivery using various microneedle (MN) applications. (A) Corneal drug delivery using MN maximizing drug loading ability with fenestrated reservoir [114] (scale bar = 200 μm) Copyright (2016) Elsevier. (B) Dissolving MN platform delivered besifloxacin to the corneal tissue [116] (scale bar = 500 μm) Copyright (2017) Springer Nature. (C) Coated MN pen applicator (MNP) for corneal drug delivery to treat angiogenesis [77] (scale bar = 100 μm) Copyright (2015) Elsevier. (D) Detachable hybrid MN pen (d-MNP) that has a bio-degradable drug-tip containing a drug for sustained corneal drug delivery for keratitis treatment [79] (scale bar = 100 μm) Copyright (2018) Elsevier. (E) Suprachoroidal space (SCS) MN injection for delivering liquid drug formulations to the posterior segment of eye [119] (scale bar = 500 μm) Copyright (2017) Springer Nature. (F) Coated MN assisted by pen applicator for the posterior segment drug delivery [78] (scale bar = 500 μm) Copyright (2018) Elsevier. (G) Tower MN (ultra-high aspect ratio) for intravitreal injection [122] Copyright (2012) John Wiley and Sons. All figures were adopted with permission.
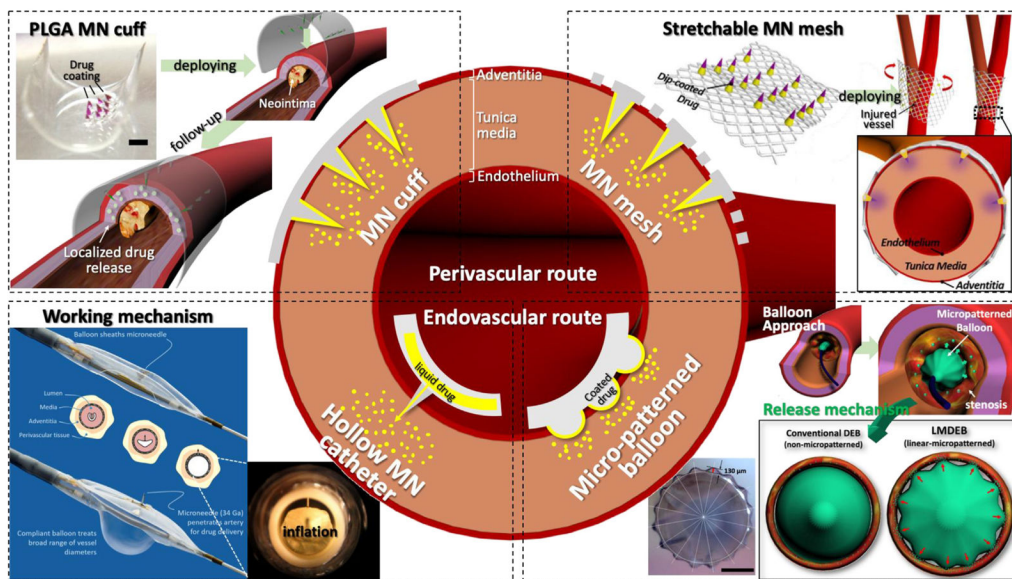
Fig. 7.

Illustration of the structure of blood vessels and overview of perivascular and endovascular drug delivery applications. Two different applications of perivascular drug delivery have been developed: 1)Biodegradable poly(lactic-co-glycolic) acid (PLGA) microneedle (MN) cuff [51] (scale bar = 1 mm) Copyright (2014) Elsevier and 2)Wrappable MN mesh [38] Copyright (2017) Elsevier. In addition, two types of endovascular drug delivery have been conducted: 1) Catheter-based hollow MN for drug infusion to the tunica media called Bullfrog® from Mercator Medsystems Inc. (image courtesy of Mercator Medsystems Inc.) and 2) Linear micropattern drug eluting balloon (LMDEB) with enhanced contact force between drug-coated surface and lumen surface (scale bar = 1 mm) [132]. All figures were adopted with permission.
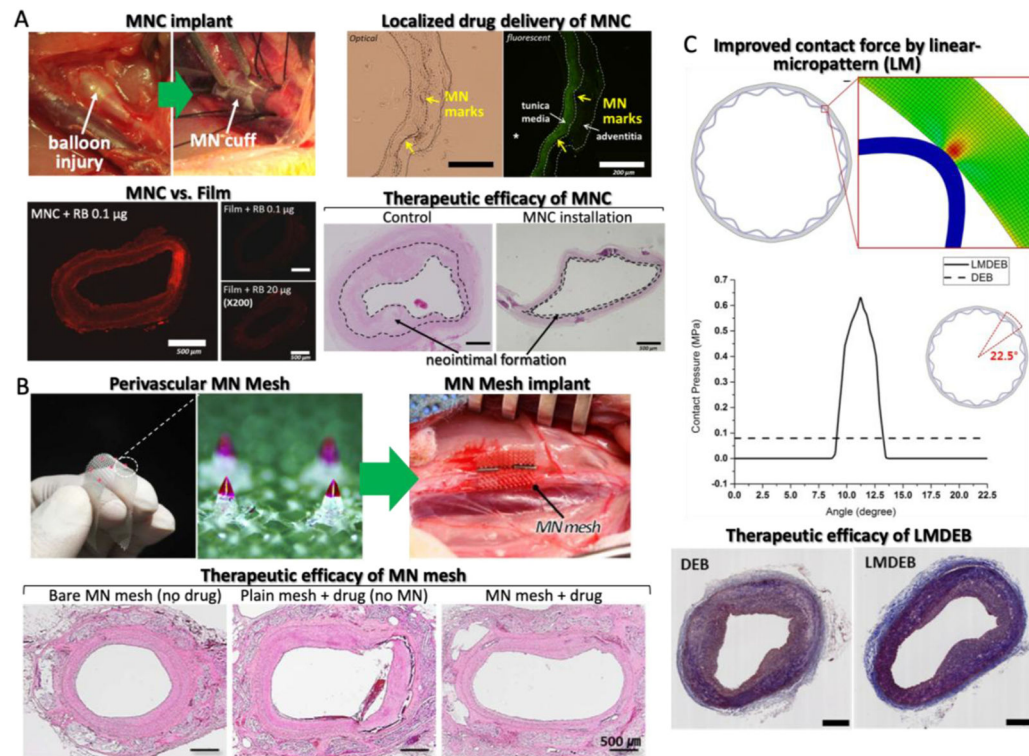
Fig. 8.

Vascular drug delivery using various microneedle (MN) applications. (A) Perivascular biodegradable MN cuff for localizing drug distribution within media layer of blood vessel [51] Copyright (2014) Elsevier. (B) Wrappable MN mesh to be more compatible with vessel environment [38] Copyright (2017) Elsevier. (C) Linear micropatterned drug eluting balloon (LMDEB) with improved contact force by micropatterns onto balloon surface [132] (scale bar = 500 μm). All figures were adopted with permission.
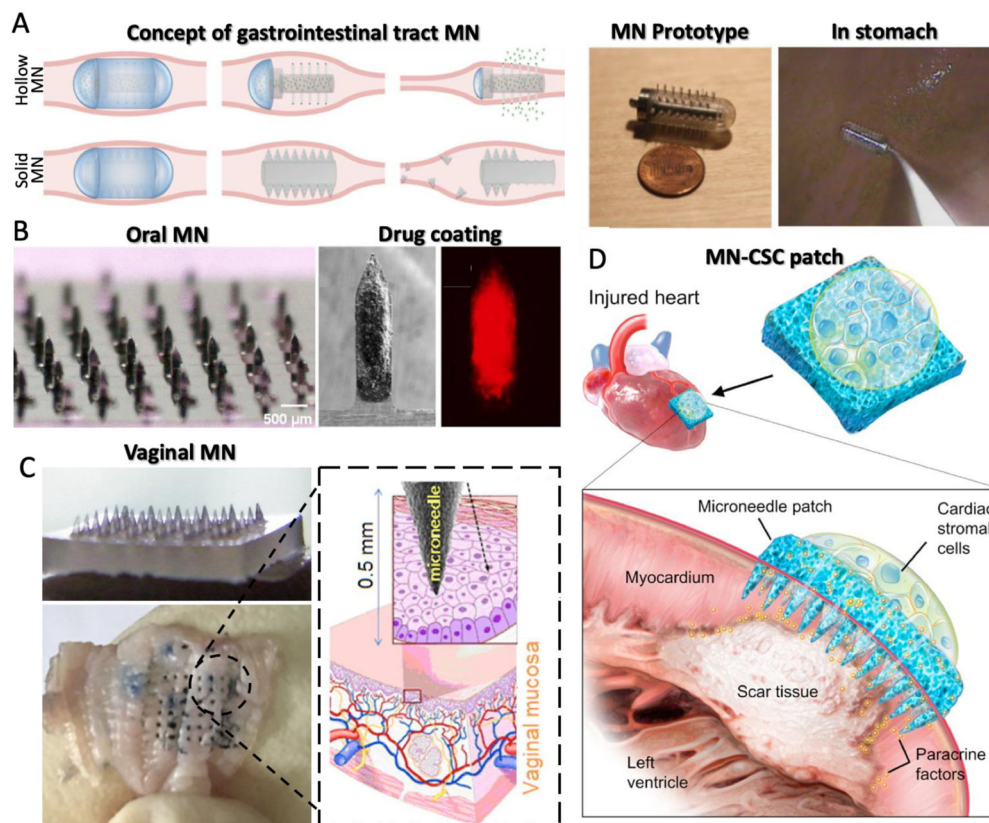
Fig. 9.
(A) Concept and prototype of microneedle (MN) capsule for gastrointestinal tract drug delivery [133] Copyright (2015) Elsevier. (B) Drug-coated MN array for treating oral cavity [134] Copyright (2015) Springer Nature. (C) MN array to vaginal drug delivery application [140] Copyright (2017) Elsevier. (D) Cardiac stromal cell-delivering MNs for heart regeneration [141] Copyright (2018) AAAS. All figures were adopted with permission.

Table 1

Physicochemical characteristics of various MNs for non-transdermal target tissues.

Target tissue	Size & shape L = length AR = aspect ratio	Material & type	Drug & release	Fabrication	Application	Ref.
Rabbit cornea	L:400–750 pm AR: 2.6–3.0	Metal Coated	DNA, Bevacizumab Instant delivery	Laser-cutting (2D cut)	Manual patching	[22][113]
Human cornea	L: 961 ±27 pm AR: 2.4–2.8	PVA/PVP Dissolving	Besifloxacin Sustained (< 24 h)	Conventional molding	Manual patching	[116]
Mouse cornea	L: 500 pm AR: 2.0	MeHA/HA Double layered	Immunoglobulins Sustained (> 1 day)	Multiple molding	Manual patching	[117]
Mouse cornea	L: 140 pm AR: 0.7	SU-8 Coated	Sunitinib Instant delivery	Transfer molding	Pen-type injector	[77]
Mouse cornea	L: 150 pm AR: 1.5	SU-8/PLGA Hybrid	PHMB Sustained (< 4 day)	Transfer molding	Pen-type injector	[79]
Pig choroid	L: 750–1000 pm AR: 2.5–3.5	Glass or Metal Hollow	Bevacizumab Instant injection	Conventional machining	Syringe	[119] [120] [121]
Beagle sclera	L: 400 pm AR: 1.5	SU-8 Coated	Rhodamine B (dye) Instant delivery	Transfer molding	Pen-type injector	[78]
Rabbit sclera	L: 5–10 mm AR: ultra-high	Nickel Hollow	Phenylephrine Instant injection	Drawing lithography	Syringe	[122]
Canine aorta	L: 600–700 pm AR: 2.2–2.7	PLGA Coated	Paclitaxel Sustained (<4wks)	Thermal drawing	Surgery (Cuffed base)	[110] [49]
Rabbit aorta	L: 650 pm AR: 3.5	PLGA Coated	Paclitaxel Sustained (<4wks)	Thermal drawing	Surgery (Cuffed base)	[50][51]
Rabbit aorta	L: 650 pm AR: 3.5	PLGA Coated	Paclitaxel/Sirolimus Sustained (<4wks)	Thermal drawing	Surgery (Cuffed base)	[129]
Rabbit aorta	L: 640 pm AR: 1.5	PLGA Coated	Sirolimus Sustained (<4wks)	Transfer molding	Surgery (Mesh base)	[38]
Human Aorta	L: 900 pm AR: 2.6–3.0	Metal Hollow	Dexamethasone Instant injection	Conventional machining	Intervention (Catheter)	[130] [131]
Pig GI tract	L: 5 mm AR: 25G needle	Metal Hollow	Insulin Instant delivery	Conventional assembly	Orally (Pill type)	[133]

Target tissue	Size & shape L = length AR = aspect ratio	Material & type	Drug & release	Fabrication	Application	Ref.
Porcine buccal tissue	L: 700 pm AR: 3.5	Metal Coated	Doxorubicin Instant delivery	Laser-cutting (2D cut)	Manual patching	[134] [137]
Human vagina	L: 650 pm AR: 1.8	Compounds Dissolving	Biological agents Instant delivery	Conventional molding	Manual patching	[139]
Mouse vagina	L: 650 pm AR: 1.8	Compounds Dissolving	Biological agents Instant delivery	Conventional molding	Manual patching	[140]
Cardiac muscle	L: 600 pm AR: 2.0	PVA Porous	Cardiac cell Instant delivery	Conventional molding	Surgery	[141]